Normal and High-Strength Continuously Wound Ties

University of Cincinnati
Department of Civil and Architectural Engineering and Construction Management

Malory R. Gooding
Elizabeth A. Mosier
Bahram M. Shahrooz, PhD, PE, FACI, FASCE, FACI

CHARLES PANKOW FOUNDATION
Building Innovation through Research

Table of Contents

List of Tables

List of Figures

Abstract

Advancements in steel reinforcement bending machines have allowed for the fabrication of continuously wound ties (CWTs), which are constructed from a single piece of reinforcement. CWTs are being used in place of conventional transverse reinforcement in concrete compression members to reduce waste and speed the construction process. CWTs are also expected to enhance the performance of special seismic compression members (a) due to anticipated improved confinement of the compressed concrete core and (b) because most legs of CWTs do not rely on hooks for development. Special boundary elements (SBEs) of structural walls are an example of a member that can benefit from the use of CWTs.

A total of twenty reduced scale SBEs were fabricated and subjected to uniaxial, monotonically increasing axial compression to evaluate the performance of members reinforced with CWTs. All the specimens reached and exceeded axial compressive strength capacity calculated using the measured material properties and ignoring the reduction factor of 0.80 that accounts for unintended eccentricity. The specimens confined with CWTs exhibited improved post-peak ductility in comparison to those employing conventional ties. However, all the current ACI requirements for transverse reinforcement must be satisfied to take full advantage of enhanced post-peak ductility offered by CWTs. Post-peak ductility was found to be further enhanced by utilizing Gr. 80 CWTs in conjunction with 10 ksi concrete.

Acknowledgments

The project was guided by the Industry Advisory Panel consisting of Dr. Jack Moehle from the University of California at Berkeley, Mr. Neal Anderson from SGH, and Dr. Reza Bayat from Englekirk. The Industry Champion for the project was Mr. Ron Klemencic, Chairman and CEO of MKA. These individuals are recognized and thanked for their advice and guidance during the project to ensure the test program provides results that are usable to industry practice.

Material donations along with technical support of the following companies are gratefully acknowledged: Janell Concrete and Masonry Equipment, Dayton Superior, Contractors Materials Co. (CMC), Alamillo, Nucor (Harris Rebar), Commercial Metals Company (CMC), and Pacific Steel Group.

The assistance of the laboratory staff at the Pacific Earthquake Engineering Research Center at the University of California at Berkeley was crucial to complete the testing program. Danis Construction is thanked for facilitating and assisting the fabrication of phase 1 specimens. The following students at the University of Cincinnati are sincerely acknowledged for their help in various aspects of fabricating the test specimens and installing many strain gages in each specimen: graduate students Sushil Kunwar and Charlie Tamayo, and undergraduate research assistants Ambar Alvarez-Garcia and Samuel Blesi.

Symbols

A_{ch}	=	cross-sectional area of a member measured to the outside edges of transverse reinforcement
A_{core}	=	area of the concrete core, calculated as the area bound by the centerlines of the edge longitudinal reinforcement
A_g	=	gross area of concrete section
A_{sh}	=	total cross-sectional area of transverse reinforcement, including crossties, within spacing s and perpendicular to dimension b_c
A_{st}	=	total area of longitudinal reinforcement
b	=	width of compression face of member
b_c	=	cross-sectional dimension of member core measured to the outside edges of the transverse reinforcement composing area A_{sh}
d_b	=	nominal diameter of bar, wire, or prestressing strand
E_c	=	modulus of elasticity of concrete
f_c	=	stress in concrete corresponding to a specific strain during an axial compression test
f_l	=	uniform confinement pressure (terminology used by Saatcioglu and Razvi, 1992)
f_{le}	=	equivalent confiding pressure (terminology used by Saatcioglu and Razvi, 1992)
f'_c	=	specified compressive strength of concrete, usually obtained from standard cylinder test
f'_{cc}	=	in-place compressive strength of confined core concrete in column
f'_{co}	=	in-place compressive strength of unconfined concrete in column
f'_l	=	lateral confinement pressure from transverse reinforcement
f_s	=	stress in reinforcement
f_t	=	maximum experimentally inferred stress in transverse reinforcement
f_u	=	ultimate tensile strength of reinforcement
f_y	=	specified or measured yield strength of reinforcement
f_{yt}	=	specified yield strength of transverse reinforcement
h	=	depth of compression face of member
h_x	=	maximum center-to-center spacing of longitudinal bars laterally supported by corners of crossties or hoop legs around the perimeter of the column
k_e	=	effective confinement index
k_f	=	concrete strength factor
k_n	=	confinement effectiveness factor
P_c	=	load carried by the concrete with longitudinal steel contribution removed
P_{max}	=	maximum axial load applied during an axial compression test
P_o	=	nominal axial strength at zero eccentricity, defined by ACI 318-19 Equation 22.4.2.2 unless noted otherwise
P_u	=	factored axial force; to be taken as positive for compression and negative for tension
s	=	spacing of transverse reinforcement in longitudinal direction
ε_{01}	=	concrete compressive strain at f'_c (terminology used by Saatcioglu and Razvi, 1992)
ε_{085}	=	concrete compressive strain at $0.85f'_c$ (terminology used by Saatcioglu and Razvi, 1992)
ε_1	=	concrete compressive strain at f'_{cc} (terminology used by Saatcioglu and Razvi, 1992)
ε_{20}	=	concrete compressive strain at $0.20f'_{cc}$ (terminology used by Saatcioglu and Razvi, 1992)

ε_{85}	=	concrete compressive strain at $0.85f'_{cc}$ (terminology used by Saatcioglu and Razvi, 1992)
ε_c	=	strain in concrete corresponding to a specific stress during an axial compression test
ε_{cc}	=	concrete compressive strain at f'_{cc} (terminology used by Mander et al., 1988)
ε_{co}	=	concrete compressive strain at f'_{co} (terminology used by Mander et al., 1988)
ε_{cu}	=	ultimate confined concrete strain, defined as concrete strain at first hoop fracture (terminology used by Mander et al., 1988)
ρ_s	=	volumetric ratio of transverse reinforcement, defined as volume of transverse steel within spacing s divided by volume of concrete, A_{ch} multiplied by s, unless noted otherwise. This variable is defined differently in several literature sources

Abbreviations

ACI	American Concrete Institute
CWT	Continuously wound tie
HSC	High-strength concrete
HSR	High-strength reinforcement
NSC	Normal-strength concrete
NSR	Normal-strength reinforcement
OBE	Ordinary boundary element
PEER	Pacific Engineering Earthquake Research Center
SBE	Special boundary element
SMFC	Special moment frame column
xSBE	Enhanced special boundary element

Chapter 1 Background

1.1 Introduction

Concrete subjected to triaxial compressive stress has enhanced strength and ductility compared to concrete under uniaxial compression. It is well known that compressive strength and ductility of concrete passively confined by transverse reinforcement is superior to unconfined concrete. As axial compressive load is applied to a concrete member, the member shortens and expands laterally due to Poisson's effect. The expansion is minimal until concrete approaches its axial compressive strength (around $0.9f'_c$) at which point internal cracking and, hence, lateral expansion increases. At this point, passive confinement from transverse reinforcement is activated, leading to enhanced strength and ductility of the confined concrete core. Additionally, transverse reinforcement enhances shear and torsional strength.

Conventional steel reinforcing ties have been an effective passive confinement. Several initiatives are underway to reduce waste and speed the construction process, one of which is to use continuously wound ties (CWTs) in place of conventional steel reinforcing ties in concrete compression members. CWTs can refer to two types of tie reinforcement: (1) a helical made from a single piece of reinforcing bar (Figure 1.1); or (2) a single hoop with multiple legs wound from a single piece of reinforcing bar (Figure 1.2). This research project focuses on the latter.

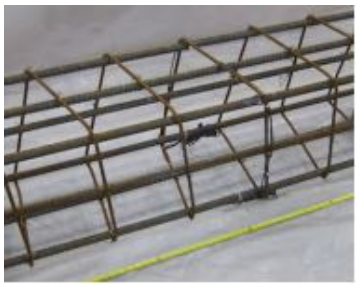

Figure 1.1 Continuously wound helix (Shahrooz et. al, 2016)

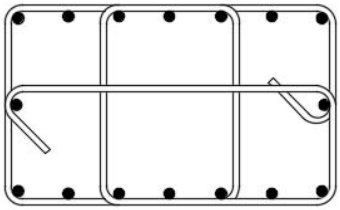

Figure 1.2 Continuously wound tie

CWTs are expected to improve tie anchorage and confinement of the concrete core which increases ductility of critical reinforced concrete compression members, particularly by enhancing inelastic seismic response of members subjected to high moment and axial loads. Such members are columns of special moment frames (SMFCs) and special boundary elements (SBEs) of walls. Test specimens for this project are detailed based on ACI 318-19 provisions for SBEs of walls, since they are more prevalent in practice compared to SMFCs.

Members reinforced with CWTs are expected to have enhanced performance because of several reasons, such as:

1. Most legs do not rely on hooks for development.
2. The tie is continuous rather than consisting of separate components. Therefore, concrete confinement, seismic performance, and post failure response should be enhanced.

CWTs require fewer individual pieces of reinforcing bar and 135-degree seismic hooks than conventional tie assemblies. Seismic hooks are difficult to place in the field. Additionally, the hooks increase congestion in already heavily reinforced column and wall sections. Utilizing CWTs may reduce construction costs and tie placement time in some situations. Benefits of CWTs are expected to be enhanced if fabricated with high-strength reinforcing bars (HSR) in conjunction with high-strength concrete (HSC). Enhanced performance is expected because HSC is more brittle and, thus, requires higher confinement pressure to achieve post-peak ductile behavior in comparison to normal strength concrete (NSC).

Due to the lack of experimental and/or field data on the performance of CWTs, the American Concrete Institute (ACI) 318 Building Code does not currently account for the potential benefits of CWTs and treats them similar to conventional reinforcement. With their growing use in practice, physical testing is required to understand behavior of members reinforced with CWTs and compare their performance with conventionally reinforced members. CWTs are expected to be beneficial when utilized in special seismic systems, specifically SBEs and SMFCs. Both of these systems are designed to achieve inelastic behavior under seismic demands. It is critical to understand the stress-strain relationships and inelastic response of members reinforced with CWTs to ensure safety and adequate performance of structural systems. Additionally, tests are needed to see if CWTs enhance performance of HSC with HSR or normal-strength reinforcement (NSR). With enhanced performance, the stringent ACI 318 provisions for confinement of SBEs could potentially be relaxed for members reinforced with CWTs.

1.2 Objectives of Research Program

The primary objective of the reported study was to identify and quantify potential strength and strain capacity enhancements from utilizing CWTs instead of conventional reinforcement. Furthermore, stress-strain relationship of concrete confined by CWTs was to be obtained and compared with existing models developed for conventional transverse reinforcement. Reliable moment-curvature relationships, which depend on modeling of confined concrete, are a key component of nonlinear dynamic analysis required for performance-based design. The overarching goal was to examine potential changes, if any, to ACI 318-19 code reflecting research results.

1.3 Overview of Research Program

A total of twenty reduced scale SBEs were fabricated and subjected to uniaxial, monotonically increasing axial compression to evaluate the performance of members reinforced with CWTs. The geometry and reinforcing ratios in the test specimens were typical of industry practice for high rise construction. The test specimens were reinforced with normal-strength reinforcement (NSR) ASTM A 706 Grade 60 and high strength reinforcement (HSR) ASTM

A706 Grade 80. Both normal-strength concrete (NSC) and high-strength concrete (HSC) were utilized with design compressive strengths, f'_c, of 6 ksi and 10 ksi, respectively. The research program was completed in two phases, with the results and observations from the first phase informing the selection of the test variables for the second phase specimens.

1.4 ACI 318 Code Provisions

ACI 318 governs the design and detailing of confined concrete members. Relevant provisions to the detailing of transverse reinforcement in SBEs are reviewed in this section. Although the focus of this project is concrete confined by CWTs in SBEs, relevant provisions for SMFCs are also summarized in this section.

1.4.1 Permitted grades of reinforcement for special seismic systems

ACI 318-19, Table 20.2.2.4a outlines permitted reinforcement grades and maximum yield strength allowed for calculations based on reinforcement function. The table permits the use of A615, A706, A995, A996, and A1035 reinforcing bars with a maximum permitted yield strength of 100 ksi for lateral support of longitudinal reinforcement, i.e., concrete confinement in special seismic systems. For flexure and axial force resistance in special seismic systems, the maximum yield strength permitted is limited to 100 ksi for ASTM A706 and 60 ksi for ASTM A615. ASTM A615 is allowed with the following additional exceptions:

1. Yield from mill tests must not exceed f_y by more than 18 ksi.
2. Ratio of actual tensile strength to actual yield strength must be at least 1.25.
3. Minimum elongation in 8 in. must be at least 14% for No.3 to No. 6, at least 12% for No.7 to No.11, and 10% for No.14 to No.18.

1.4.2 Buckling and confinement

ACI 318-19 has three provisions related to concrete confinement and buckling of longitudinal reinforcement. These provisions are summarized in this section.

1.4.2.1 ACI section 18.7.5.3

This section requires that the spacing of transverse reinforcement must be the least of (a) through (d) shown below. Provision (a) is to ensure adequate concrete confinement, while provisions (b), (c), and (d) are intended to control longitudinal bar buckling.

(a) $b/3$
(b) $6d_b$ for Grade 60 longitudinal reinforcement
(c) $5d_b$ for Grade 80 longitudinal reinforcement
(d) $s_o = 4 + \left(\frac{14 - h_x}{3}\right)$ with $4 \leq h_x \leq 6$

In provision (d), h_x is the spacing of supported longitudinal bars (see Figure 1.1). Per ACI 318-19 Section 18.10.6.4 (e), h_x is not to exceed the lesser of 14 in. or 2/3 times the boundary element thickness. At least every other longitudinal bar must be supported.

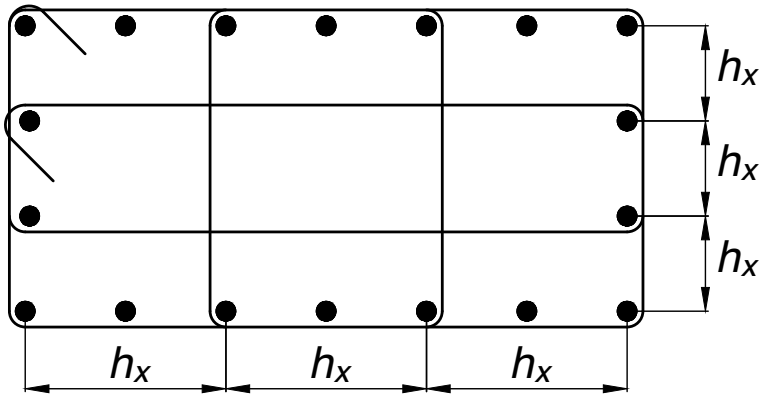

Figure 1.3 Definition of h_x

1.4.2.2 ACI table 18.10.6.5b

This table provides maximum vertical spacing of transverse reinforcement for SBEs based on the grade of the primary flexural reinforcement bar. The limitation is intended to prevent buckling of longitudinal reinforcing bars until strains from reversed cyclic seismic loading reach inelastic range. A smaller spacing of transverse reinforcement is required to obtain similar performance between longitudinal HSR and NSR. A subset of ACI Table 18.10.6.5b is provided below.

Grade of primary flexural reinforcement	Maximum vertical spacing of transverse reinforcement	
60	Lesser of:	6 d_b
		6 in.
80	Lesser of:	5 d_b
		6 in.
100	Lesser of:	4 d_b
		6 in.

1.4.2.3 ACI table 18.10.6.4(f)

Table 18.10.6.4(f) provides equations for transverse reinforcement ratio, A_{sh}/sb_c, to ensure proper concrete confinement. The provisions are similar to those in Table 18.7.5.4 for SMFC confinement except equation (c), repeated as Eq. 1.3 below, is not included for SBEs. Eq. 1.3 is required for SMFCs when $f'_c > 10{,}000$ psi or $P_u > 0.3A_g f'_c$. For SBEs reinforced with rectilinear hoops, the area ratio of transverse reinforcement, A_{sh}/sb_c, must be the greater of (a) and (b). Provision (a) (Eq. 1.1) is intended to provide adequate confinement reinforcement so that compressive strength can be maintained after spalling for slender elements where cover accounts for a large portion of the concrete gross area. Provision (b) (Eq. 1.2) is intended to provide sufficient reinforcement for adequate confinement of thick walls where cover does not account for a significant portion of the wall thickness.

(a) $0.3\left(\frac{A_g}{A_{ch}}\text{-}1\right)\frac{f'c}{f_{yt}}$ **Eq. 1.1**

(b) $0.09\frac{f'c}{f_{yt}}$ **Eq. 1.2**

(c) $0.2k_f k_n \frac{P_u}{f_{yt}A_{ch}}$ **Eq. 1.3**

1.5 Summary of Previous Research on Concentric Axially Loaded Columns

Extensive research has been conducted on square columns under concentric axial compression. Goals of past research were to determine properties of concrete confined by transverse reinforcement and develop stress-strain models for confined concrete. Some of the test programs on NSC and HSC are summarized in this section to better understand the behavior of confined concrete.

1.5.1 Normal strength concrete

Sheikh and Uzumeri (1980) tested twenty-four square columns. Concrete and steel strengths were approximately 5 ksi and 60 ksi, respectively. Every longitudinal bar of the columns was supported. Tie steel consisted of plain bar with yield strength ranging between 40 and 100 ksi. Volumetric ratio of transverse reinforcement, ρ_s, varied between 0.8% to 2.4%. The researchers observed that well distributed transverse reinforcement enhanced the strength and ductility of confined concrete. The ratio of P_{max}, the maximum applied axial load, to P_o, the unconfined compression strength, varied between 0.96 to 1.16. It was concluded that for a constant ρ_s, decreasing the vertical tie spacing (thus requiring smaller diameter ties) increases strength and ductility even though the tie stiffness is decreased.

Scott, Park, and Priestley (1982) tested twenty-five square columns. Longitudinal bars were each supported by a rectilinear tie leg and had a yield strength of either 40 ksi or 55 ksi. Ties were all plain round bar with a 40 ksi yield strength. Volumetric ratio of transverse reinforcement, ρ_s, varied between 1.4% to 3.09%. Concrete strength was 3.6 ksi. The researchers reported that specimens subjected to concentric monotonic loading exhibited significant strength gain, around 20%, and good ductility. The researchers concluded that increasing the tie size while increasing tie spacing to maintain constant ρ_s reduced confinement efficiency. Increase in the tie volumetric ratio enhanced peak concrete core stress and strain at the first hoop fracture and decreased the descending slope of the core stress-strain curve.

Moehle (1985) tested ten half-scale reinforced concrete columns. Transverse reinforcement layouts are shown in Figure 1.4. Mean concrete strength was 4.9 ksi, and all steel reinforcement was Grade 60. Volumetric ratio of transverse reinforcement, ρ_s, was 2.07%, 1.82%, and 1.21% for configurations "A", "B" and "C", and "D", respectively, and s/d_b was 2.0. Figure 1.5 shows load-deflection relationships for the test specimens. Specimens with every longitudinal bar supported performed in a more ductile manner and reached higher strengths than specimens without intermediate longitudinal bar support. Additionally, specimens with 180-degree intermediate hooks showed slight improved post-peak response compared to specimens with 135-degree and 90-degree alternating hooks.

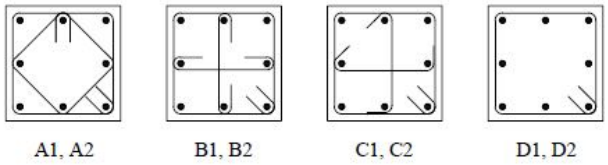

Figure 1.4 Test specimen configurations (Moehle, 1985)

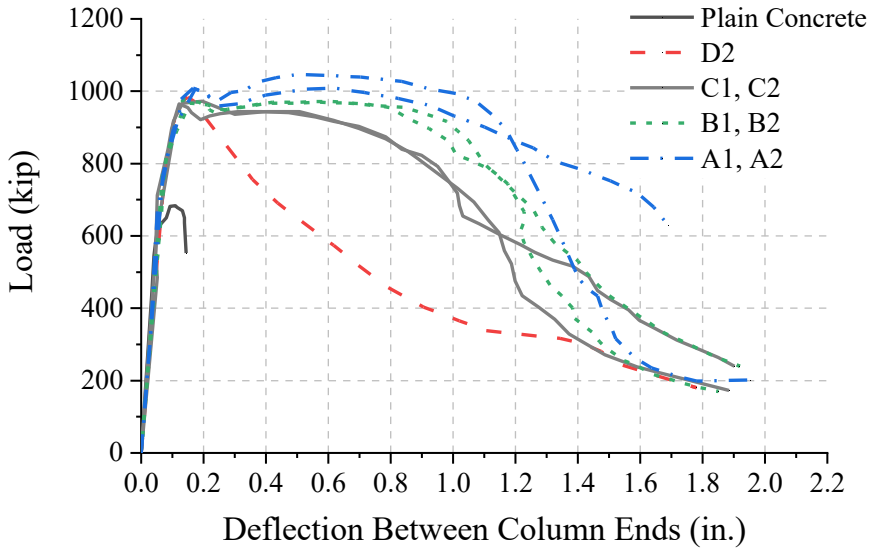

Figure 1.5 Measured load-deflection curves (adopted from Moehle, 1985)

1.5.2 High strength concrete

Cusson (1994) tested twenty-seven HSC columns. Concrete strength varied from 8.7 ksi to 17 ksi. Columns had Grade 60 longitudinal bars, each supported by a rectilinear tie or crosstie. Transverse reinforcement had a yield strength of either 58 ksi or 102 ksi. Volumetric ratio of transverse reinforcement, ρ_s, ranged from 1.4% to 4.9%, and s/d_b ranged from 1.98 to 8.85. Cusson (1994) reported that the concrete cover spalled abruptly resulting in axial capacity loss. Post spalling, the ties provided passive confinement which resulted in increased ductility. Well confined specimens reached a second peak strength due to passive confinement. The P_{max}/P_o ratio, ratio of maximum axial load in the tests to the axial capacity per ACI 318, varied between 0.87 and 1.40 with a 0.99 average. Cusson explained that passive confinement from transverse reinforcement becomes effective later in the stress-strain curve making passive confinement from transverse reinforcement less efficient in HSC compared to NSC. The researcher points out that strength gain depends on confinement level, which in turn depends on transverse reinforcement strength. Cusson found that ties in lightly confined specimens may only reach 50% of their yield strength at failure. Therefore, HSR may not increase strength and ductility for some specimens. However, if the section is heavily confined and HSR ties yield, the use of HSR ties will increase strength and toughness compared to the use of NSR ties.

Saatcioglu and Razvi (1998) studied twenty-six HSC columns. Columns were either unreinforced or had longitudinal bars each supported by either a closed rectilinear tie or a crosstie with 135-degree hooks. Reinforcement yield strength ranged from 58 ksi to 145 ksi. Concrete strength varied between 8.7 ksi and 18 ksi. Volumetric ratio of transverse

reinforcement, ρ_s, varied between 1.4% to 4.9%, and s/d_b ratio ranged between 3.4 and 7.5. Saatcioglu and Razvi (1998) concluded that HSC could have the same strength enhancement as NSC if confinement pressure provided is proportional to concrete strength. It is clear that increase in concrete strength leads to a decrease in ductility and strength enhancement, see Figure 1.6. It was concluded that cover spalling of HSC, especially with tight reinforcement cages, could occur before the concrete unconfined compressive strength is reached. However, well confined columns reached or exceeded their unconfined compressive strengths after spalling occurred.

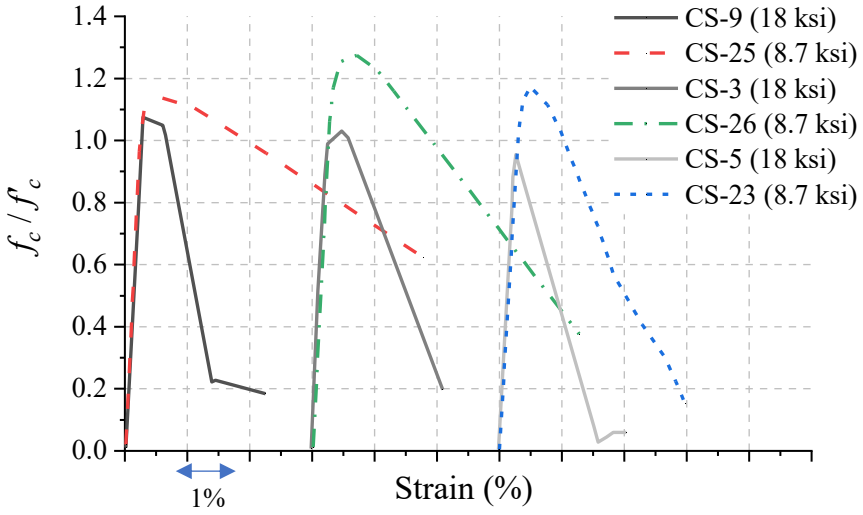

CS-9& CS-25: s/d_b = 7.5, ρ_s = 3.06%; CS-3 & CS-26: s/d_b = 3.4, ρ_s = 2.16%;
CS-5 & CS-23: s/d_b = 7.5, ρ_s = 1.32%

Figure 1.6 Normalized stress-strain curves showing effect of concrete strength on strength and deformability of specimens (adopted from Saatcioglu and Razvi, 1998)

Sharma, Pradeep, and Kaushik (2005) tested eighteen square concrete columns. Specimens had longitudinal bars each supported by a rectilinear tie leg. Volumetric ratio of transverse reinforcement, ρ_s, varied between 2.2% and 5.62%, and s/d_b ranged between 2.5 and 4.17. Transverse reinforcement had a yield strength of either 60 ksi or 75 ksi. Concrete strength utilized was either 9.0 ksi or 12 ksi. Sharma et al. (2005) observed that cover spalling led to a sudden load drop. The researchers also observed that increased confinement is required for HSC to achieve similar behavior and strength and ductility enhancements as confined NSC. A second peak strength only occurred in well-confined specimens. It was concluded that increasing tie yield strength did not have a large effect on HSC behavior since ties only yielded for well-confined specimens at the second peak strength.

1.5.3 Synthesis of NSC and HSC column tests

Multiple research programs have been reported on the behavior of confined concrete columns with NSC or HSC and either NSR or HSR. In the studies, well-confined NSC columns reached a second peak strength and exhibited excellent ductility. Though HSC columns and columns with high axial load level behaved in a more brittle manner than typical NSC columns,

well-confined HSC columns that utilized HSR exhibited behavior enhancements similar to NSC columns. SMFCs detailed to ACI 318-19 display great post-peak behavior. However, the adoption of Table 18.7.5.4, Equation (c) with the ACI 318-14 Code edition requires designers to use large quantities of transverse reinforcement, which increases cost and often causes constructability issues. Designers are moving towards structural walls with SBEs as the seismic force resisting system of choice due to the stringent SMFC requirements and the inherent redundancy of structural wall systems.

The following observations can be made based on the summarized studies:

1. Most well-confined NSC columns reached a second peak strength and exhibited excellent ductility.
2. Decreasing tie size and spacing while maintaining a constant volumetric ratio of transverse reinforcement provided better ductility than increasing spacing and transverse bar size.
3. Closed hoops performed better as confining reinforcement than 135-degree hooks, which performed better than 135-degree and 90-degree alternating hooks.
4. HSC behaved in a less ductile manner than NSC, and passive confinement was less effective.
5. HSC often exhibited early cover spalling before the unconfined compressive strength was reached due to a plane of weakness at the reinforcement cage.
6. Volumetric ratio of transverse reinforcement must be increased with increasing concrete strength to achieve strength and ductility enhancements.
7. Transverse HSR increased strength and ductility in well-confined HSC specimens. However, if specimens are not adequately confined, transverse HSR will not reach yield strength.

1.6 Summary of Previous Research on Concentric Axially Loaded SBEs

Limited test data are available for wall boundary elements subjected to concentric axial compression that are compliant with ACI 318-19 SBE provisions. Many tests are either not compliant with ACI 318-19 or have enhanced detailing compared to code requirements. Additionally, no tests on SBE specimens detailed with HSC and HSR could be found in the available literature. Important test programs will be reviewed and synthesized in the following sections.

1.6.1 Experimental test programs

Mander, Priestley, and Park (1988) tested sixteen half-scale rectangular specimens representing the flange region of a typical core wall. See Figure 1.7 for specimen details. Steel and concrete strengths were around 45 ksi and 6.0 ksi or 4.0 ksi, respectively. Volumetric ratio of transverse reinforcement, ρ_s, ranged from 1.62% to 7.87%, and s/d_b ranged from of 2.1 to 6. Mander et al. (1988) concluded that increasing the volumetric ratio of transverse reinforcement increased peak strength and decreased post-peak strength degradation, see Figure 2 6. The ratio of confined core stress, $f'_{cc,}$ to unconfined core stress, f'_{co}, exceeded 1.5 for all reinforced

specimens. It should be noted that the longitudinal bar support pattern, tie spacing, and tie volumetric ratios are enhanced compared to the ACI 318-19 SBE requirements.

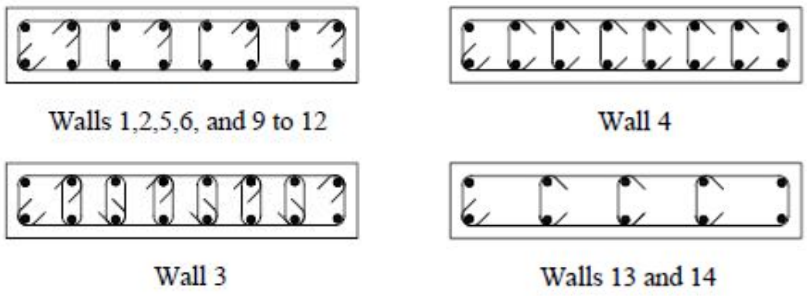

Figure 1.7 Specimen details (Mander et al., 1988)

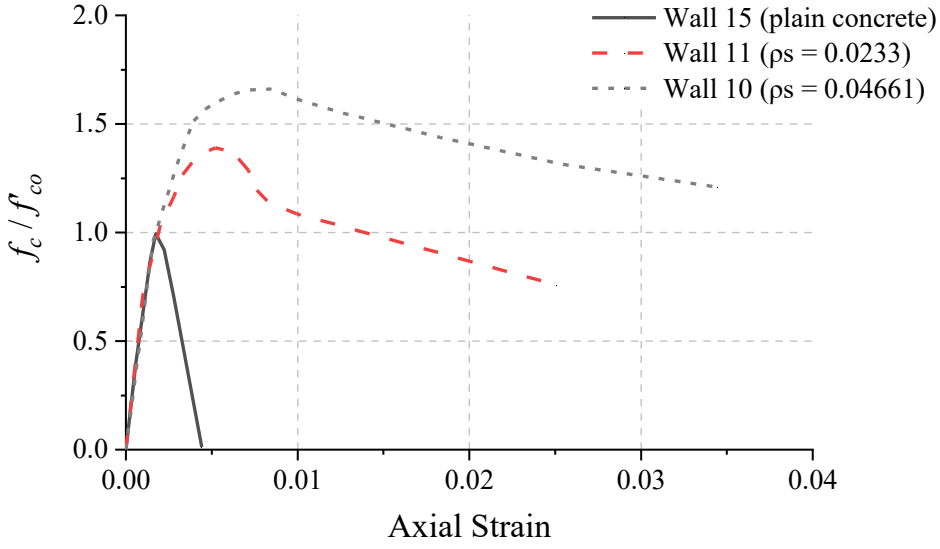

f_c = longitudinal concrete stress

f'_{co} = compressive strength of unconfined concrete

ρ_s = volumetric ratio of transverse reinforcement

Figure 1.8 Influence of volumetric ratio of transverse reinforcement (adopted from Mander et al., 1988)

Massone, Polanco, and Herrera (2014) tested twenty-four boundary elements to both reproduce the wall boundary element failures observed during the 2010 Chile Earthquake and evaluate the performance of boundary elements with improved confinement. Concrete strength was 5.7 ksi, longitudinal reinforcement yield strength 69 ksi, and transverse reinforcement yield strength was 72 ksi. Volumetric ratio of transverse reinforcement, ρ_s, varied between 2.0% and 3.8%, and s/d_b ratio was 5.55. The researchers reported that specimens reinforced with crossties having 135-degree hooks on each end had little enhancement compared to specimens reinforced with crossties with alternating 135-degree and 90-degree hooks. The ratio of confined concrete stress to unconfined concrete cylinder stress, f'_{cc}/f'_c, was typically below 1.2, and specimens did not exhibit a second peak compressive strength. Specimens displayed longitudinal bar buckling over several transverse tie spacings.

Areta and Moehle (2015) tested seven "thin" SBE specimens to see if boundary elements detailed to ACI 318-11 could achieve ductile performance. Concrete and steel strengths were 4 ksi and 60 ksi, respectively. Every other longitudinal bar was supported by a tie leg with h_x varying between 7 in. and 10 in. Transverse reinforcement consisted of a perimeter rectilinear tie and crossties with either a 135-degree seismic hook on each end or alternating 135-degree and 90-degree hooks. Transverse reinforcement ratio, A_{sh}/sb_c, varied between 1.10% to 4.65%, and s/d_b was either 3.2, 4.0, or 4.6. Areta and Moehle (2015) concluded that specimens designed per ACI code did not achieve a ductile response, see Figure 2 7. The researchers suggested that specimens could have experienced brittle axial failure due to longitudinal bar buckling and concrete cover spalling. The researchers asserted that increasing transverse reinforcement ratio and decreasing horizontal and vertical tie spacing improved behavior but did not guarantee the ductile behavior expected from special seismic members. They also reported that 135-degree seismic hooks only had slight benefit over 135-degree and 90-degree alternating hooks. Areta (2015) reported that specimens with ties supporting every other longitudinal bar had issues with longitudinal bar buckling at low average strain, around 0.9%, which in turn caused core material to fail. Longitudinal bar buckling reduced the spread of plasticity along the specimen height as well as the post-spalling strength.

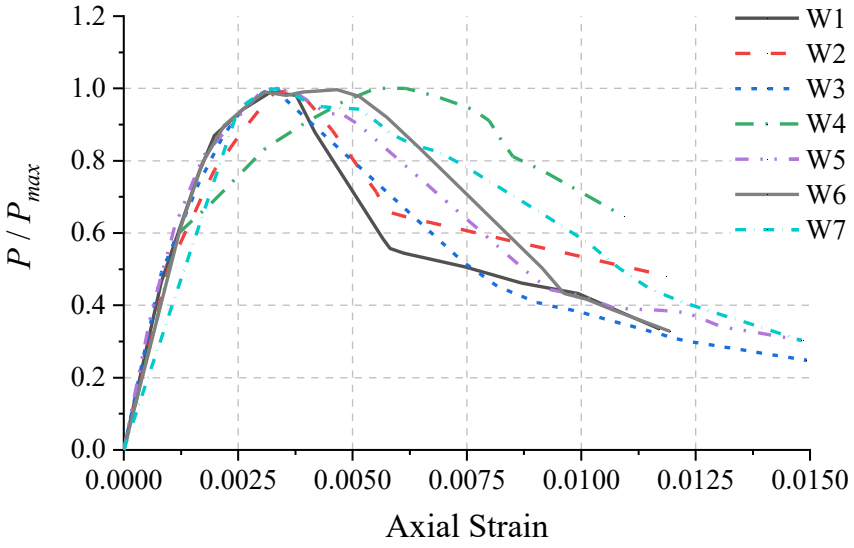

Figure 1.9 Specimen force vs. average strain relationships (adopted from Areta and Moehle, 2015)

Welt, Massone, and LaFave (2017) reported test results on twenty-two boundary elements. Longitudinal reinforcement yield strength was either 70 ksi or 80 ksi. Ties had a yield strength of either 68 ksi or 72 ksi. Transverse reinforcement ratio, A_{sh}/sb_c, varied between 0.34% and 1.76%, and the s/d_b ratio varied between 4 and 8. Several types of boundary elements were studied including NSBEs (normal boundary elements not meeting ACI 318-11 Code), OBEs (ordinary boundary elements per ACI 318-11 Code), SBEs (with every other longitudinal bar supported by ties), and xSBEs (enhanced special boundary elements exceeding ACI 318-11 SBE requirements and having every longitudinal bar supported by a tie).

Welt et al. (2017) reported that xSBE specimens with closed hoops exceeded 1% compressive strain with less than 10% reduction in peak stress. This behavior is suitable for seismic design, where flexural systems must sustain compressive load and increasing deformation while undergoing cyclic lateral load. Figure 1.10, adopted from Welt et al. (2017), shows stress-strain relationships for specimens with several different detail classifications. The researchers assert that specimens detailed as SBEs with crossties did not provide adequate longitudinal bar restraint, which led to earlier compressive failure of the specimens compared to specimens with intermediate hoops. They also concluded that restraining every longitudinal bar increased strength and deformation capacity by 30% to 100%. Welt (2015) further concluded that strength capacity is not enhanced unless s/d_b is less than 4. With s/d_b less than 4 and fully developed transverse reinforcement meeting ACI 318-14 requirements for transverse reinforcement ratio, the specimens had peak f'_{cc}/f'_c, ratio of 28-day concrete cylinder strength to peak confined concrete stress, greater than 1.5 and strain of at least 2%. Welt (2015) found that utilizing crossties rather than rectilinear hoops to support longitudinal reinforcement reduced the specimen strength, deformation capacity, and did not adequately restrain longitudinal bars against buckling.

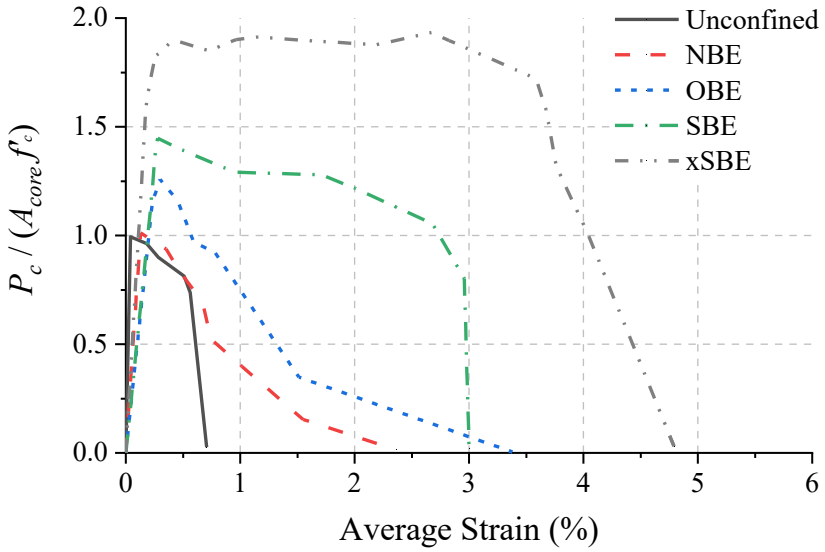

P_c = load carried by the concrete with longitudinal steel contribution removed

A_{core} = area of the concrete core, calculated as the area bound by the centerlines of the edge longitudinal reinforcement

f'_c = concrete cylinder strength

Average Strain = displacement measurement divided by gage length

Figure 1.10 Specimen stress-strain relationships (adopted from Welt et al., 2017)

Behrouzi, Welt, Lehman, LaFave, and Kuchma (2017) reviewed ACI 318-14 code provisions and performed a special wall detailing investigation. They analyzed results from Mander et al. (1988), Massone et al. (2014), and Welt (2015) to draw conclusions regarding effective SBE detailing. They concluded that a vertical spacing of transverse reinforcement of $6d_b$ yields a ratio of peak confined concrete stress to concrete cylinder stress, f'_{cc}/f'_c, of 1.25 and strain less than 1% at 20% strength loss. Tie spacing of less than or equal to $4d_b$ provides improvement, with f'_{cc}/f'_c near 1.5 and strain ranging from 1% to 4% at 20% strength loss. They

also found that volumetric ratio of transverse reinforcement greatly affects stress-strain curves of confined concrete. However, designs with volumetric ratio near the ACI 318-14 limit had limited f'_{cc}/f'_c ratios and ultimate strains, what appears to be less than 1.25 and 0.75% at 20% strength loss, respectively. The researchers recommended modifications to SBE detailing requirements to make them similar to the requirements for SMFCs, which an h_x limit of 8 in. and requirement that every longitudinal bar be supported by a tie leg.

1.6.2 Synthesis of SBE tests

Tests on code compliant isolated SBEs are limited. Tests of isolated SBEs utilizing HSC with or without HSR are almost non-existent. Available SBE tests have demonstrated that code-complaint detailing does not guarantee great post-peak performance. Since the design of many SBEs is controlled by transverse bar spacing and not every longitudinal bar is required to be supported by a tie leg, premature longitudinal bar buckling is more prevalent in SBEs than in SMFCs. However, literature has shown that enhanced detailing, such as supporting every longitudinal bar, can improve behavior, though none of the enhanced detailing is required per Code.

The following observations are made from the limited existing tests of isolated SBEs:

1. Compared to SMFCs, SBEs exhibited less strength and ductility gain due to confinement when subjected to concentric axial compression. This trend is attributed to SBE detailing provisions being relaxed compared to SMFC provisions.
2. ACI 318-14 compliant SBE specimens are not guaranteed to exhibit ductile behavior.
3. Transverse reinforcement spacing is especially critical for SBEs. Some researchers concluded that a s/d_b ratio less than 4 prevents premature longitudinal bar buckling and enhances strength and deformability.
4. Ties with hooks were inferior to closed hoops.
5. Decreasing h_x and providing support for every longitudinal bar enhanced performance.

1.7 Confined Concrete Models

This section provides a summary of three models commonly used to simulate stress-strain relationships of confined concrete. These models are Mander, Preistley, and Park (1988), Saatcioglu and Razvi (1992), and Razvi and Saatcioglu (1998). Each model is presented separately in the following subsections.

1.7.1 Mander, Preistley, and Park (1988)

Mander, Preistley, and Park (1988) developed a stress-strain model for confined concrete that can be utilized for circular or rectangular members subjected to axial compression. The model was validated with experimental research focused on circular columns and rectangular boundary elements by Mander et al. (1988) and experimental research by Scott et al. (1982) focused on square columns. The model accounts for confinement effects from rectilinear hoop reinforcement with or without intermediate ties. The model allows for different confinement pressures along each transverse axis. See Figure 1.11 for the stress-strain model in which f'_{cc} is the peak confined concrete stress and ε_{cu} is the ultimate strain defined by the first hoop fracture. The model is based on an equation presented by Popovics (1973).

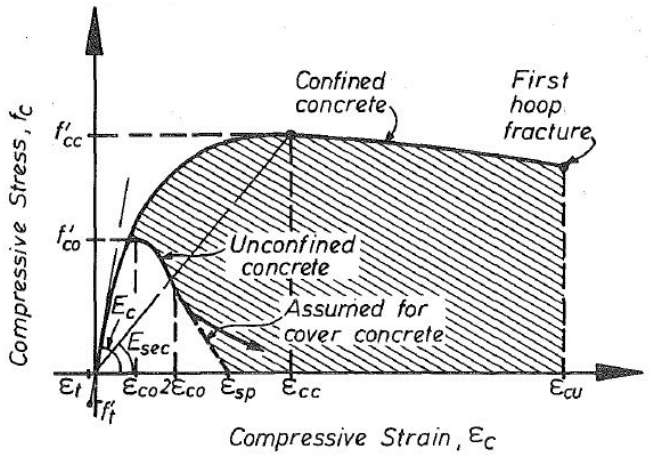

Figure 1.11 Stress-strain curve for confined concrete (Mander et al., 1988)

The model by Mander et al. (1988) utilizes a five-parameter failure surface to calculate the compressive strength of confined concrete, see Eq. 1.4. The confined concrete compressive strength is dependent on the unconfined concrete strength (f'_{co}) and the lateral confinement pressure from transverse reinforcement (f'_l). The compressive strain at peak concrete strength, ε_{cc}, is computed by considering the ratio of f'_{cc}/f'_{co} and the strain at f'_{co}. For rectangular specimens, f'_{cc} must be calculated in each principal direction and combined through the chart shown in Figure 1.12Figure 1.12. Chang and Mander (1994) developed numerical solutions for Figure 1.12.

$$f'_{cc} = f'_{co}\left(-1.254 + 2.254\sqrt{1+\frac{7.94f_l}{f'_{co}}} - 2\frac{f'_l}{f'_{co}}\right) \qquad \textbf{Eq. 1.4}$$

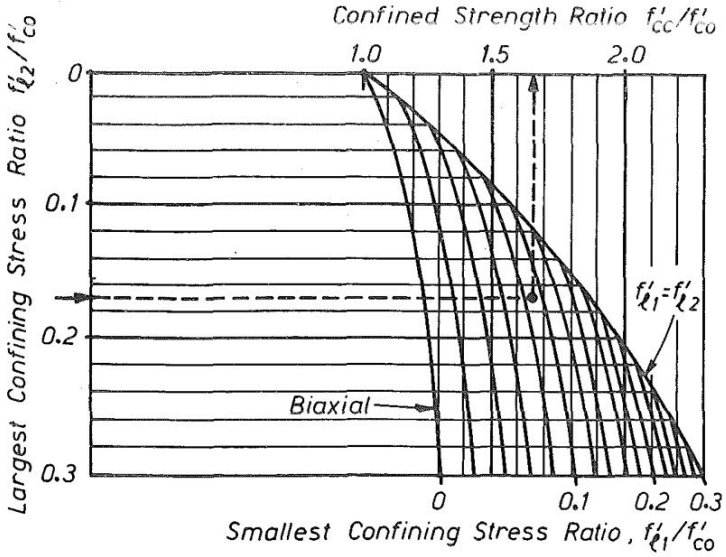

Figure 1.12 Confined concrete strength for rectangular sections (Mander et al., 1988)

The calculated lateral confinement pressure is dependent on the effective confinement index (k_e) which can be different along each principal axis for rectangular members. The confinement index is related to the clear spacing of longitudinal reinforcement, concrete core dimensions, and clear vertical spacing of transverse reinforcement. It is unclear whether the calculation of k_e should be based on the spacing of supported or unsupported longitudinal reinforcement since unsupported longitudinal reinforcement was not considered in the development of the model. For the comparisons reported herein, the spacing of supported longitudinal reinforcement was used to calculate confinement effectiveness.

1.7.2 Saatcioglu and Razvi (1992), normal strength concrete

Saatcioglu and Razvi (1992) developed a stress-strain model for confined NSC. The model is applicable to circular, square, and rectangular sections with equal or unequal confinement pressures on perpendicular faces. The model is based on a calculated equivalent uniform confinement pressure. The model was developed from square column tests by Scott et al. (1982), Razvi and Saatcioglu (1989), and Sheikh and Uzumeri (1980). The researchers used results from Mander et al. (1988) to verify the model for rectangular sections.

As seen from Figure 1.13, up to peak strain (ε_1) the stress-strain curve is represented by a parabola. The calculated peak strain increases with increasing confinement pressure and decreases with increasing unconfined concrete strength. Past peak strain, a linear descending branch is assumed down to a 20% residual strength level. To establish the descending branch, the strain at 85% of the peak confined compressive strength, ε_{85}, is estimated based on the transverse reinforcement ratio, peak confined concrete strain (ε_1), and the unconfined concrete strain at 85% strength loss (ε_{085}).

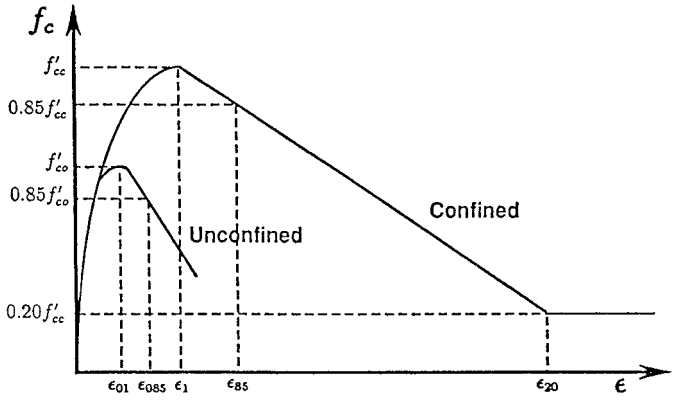

Figure 1.13 Proposed stress-strain relationship for confined concrete (Saatcioglu and Razvi, 1992)

The confined concrete strength (f'_{cc}) is calculated from Eq. 1.5 and is a function of the unconfined concrete strength (f'_{co}) plus strength enhancements from lateral confinement pressure (f_{le}). The coefficient k_1 is a function of Poisson's ratio which varies with level of lateral confining pressure.

$$f'_{cc} = f'_{co} + k_1 f_{le}$$ **Eq. 1.5**

Saatcioglu and Razvi (1992) recognized that confinement pressure is greatest at locations of high flexural rigidity, including tie levels and supported longitudinal reinforcement. Confinement pressure decreases between locations of high flexural rigidity as depicted in Figure 1.14. A uniform confinement pressure (f_l) is calculated by dividing the effective tie strength in each principal direction by the core surface area (sb_c). The calculations assume transverse reinforcement yields. The equivalent lateral pressure (f_{le}) is reduced by k_2, which accounts for confinement efficiency and decreases with increased transverse bar spacing and spacing between laterally supported longitudinal reinforcement. The equivalent lateral pressure (f_{le}) is the weighted average of the confinement pressure in each principal direction for rectangular members.

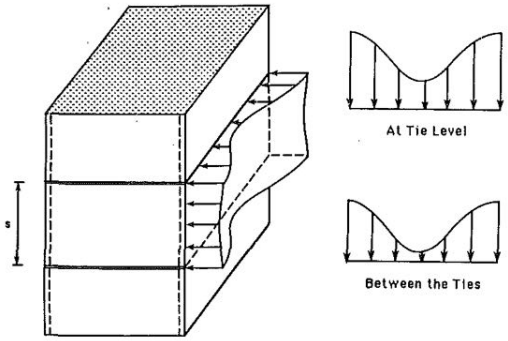

Figure 1.14 Lateral confinement pressure distribution along the length of a member (Saatcioglu and Razvi, 1992)

1.7.3 Razvi and Saatcioglu (1998), High-Strength Concrete

Razvi and Saatcioglu (1998) developed a model applicable to concrete strengths ranging between 4.5 ksi and 18.9 ksi. It is similar to the previous model (Saatcioglu and Razvi, 1992) with some modifications. The model was developed utilizing data from over 200 axial compression tests from various research programs. A diversion from the previous model is the use of the actual transverse reinforcement stress (f_s) at peak concrete stress to compute the average lateral pressure rather than assuming the steel yields. The researchers asserted that the assumption that steel yields is fairly accurate for NSC with NSR but may not be accurate for HSC reinforced with HSR. An equation was developed to calculate steel stress from regression analysis of test data, considering that the efficiency of HSR depends on concrete strength and volumetric ratio of transverse reinforcement.

The graphical representation of the model is the same as proposed by Saatcioglu and Razvi (1992). The descending branch similar to that proposed by Saatcioglu and Razvi (1992) except it is modified to be applicable for NSC, HSC, NSR, and HSR. The ε_{85} calculation was modified to include the factors k_3 and k_4 (see Eq. 1.6 and Eq. 1.7, in which f'_{co} and f_{yt} are in MPa. The k_3 factor decreases ε_{85} with increasing unconfined concrete strength. The k_4 factor increases ε_{85} with increasing steel yield strength.

$$k_3 = \frac{40}{f'_{co}} \leq 1$$ **Eq. 1.6**

$$k_4 = \frac{f_{yt}}{500} \leq 1$$ **Eq. 1.7**

The expression for the ascending branch proposed by Saatcioglu and Razvi (1992) is not applicable to high strength concrete because the experimental data indicate the initial modulus of elasticity is overestimated for such concrete. To remedy this, the researchers proposed an expression similar to that proposed by Mander et al. (1988). The exact limit of applicability of the original model by Saatcioglu and Razvi (1992) is not clear.

Chapter 2 Experimental Program

2.1 Introduction

A total of twenty reduced scale SBEs were fabricated and subjected to uniaxial, monotonically increasing axial compression to evaluate the performance of members reinforced with CWTs. The research program was completed in two phases. The results and observations from the first phase informed the selection of the test variables for the second phase specimens. The test matrix overview is shown in Figure 2.1. The test variables were as follows:

Phase 1

- Type of tie (conventional or CWT)
- Reinforcement yield strength (ASTM A706 Grade 60 or ASTM A706 Grade 80)
- Specified strength of concrete (NSC: 6000 psi or HSC: 10000 psi)
- Shape of cross section (square or rectangle)

Phase 2

- Type of tie (conventional or CWT)
- Reinforcement yield strength (ASTM A706 Grade 60 or ASTM A706 Grade 80)
- Specified strength of concrete (NSC: 6000 psi or HSC: 10000 psi)
- Lateral support of longitudinal bars (every bar or every other bar is supported)
- ACI transverse reinforcement requirements (compliant or noncompliant)

In phase 1, each specimen reinforced with CWTs had an identical counterpart reinforced with conventional ties. Three variations of transverse steel and concrete strengths were examined: (1) NSC with NSR (2 specimens), (2) HSC with NSR (4 specimens), and (3) HSC with HSR (4 specimens). Twelve specimens would be required to maintain all the paired variables. However, Phase 1 only consisted of only ten specimens. As result, the square specimens with NSC and NSR were excluded. This exclusion is deemed reasonable because wall boundary elements are usually rectangular.

All ten specimens tested in Phase 2 were rectangular, eight of which were reinforced with CWTs and the remaining two had conventional transverse reinforcement. Three variations of transverse steel and concrete strengths were also examined in the second phase: (1) HSC with NSR (4 specimens), (2) NSC with NSR (2 specimens), and (3) HSC with HSR (4 specimens). Four specimens met all the applicable ACI requirements whereas the remaining six specimens did not. In seven specimens every longitudinal bar was laterally supported, and every other longitudinal bar was laterally supported in three specimens.

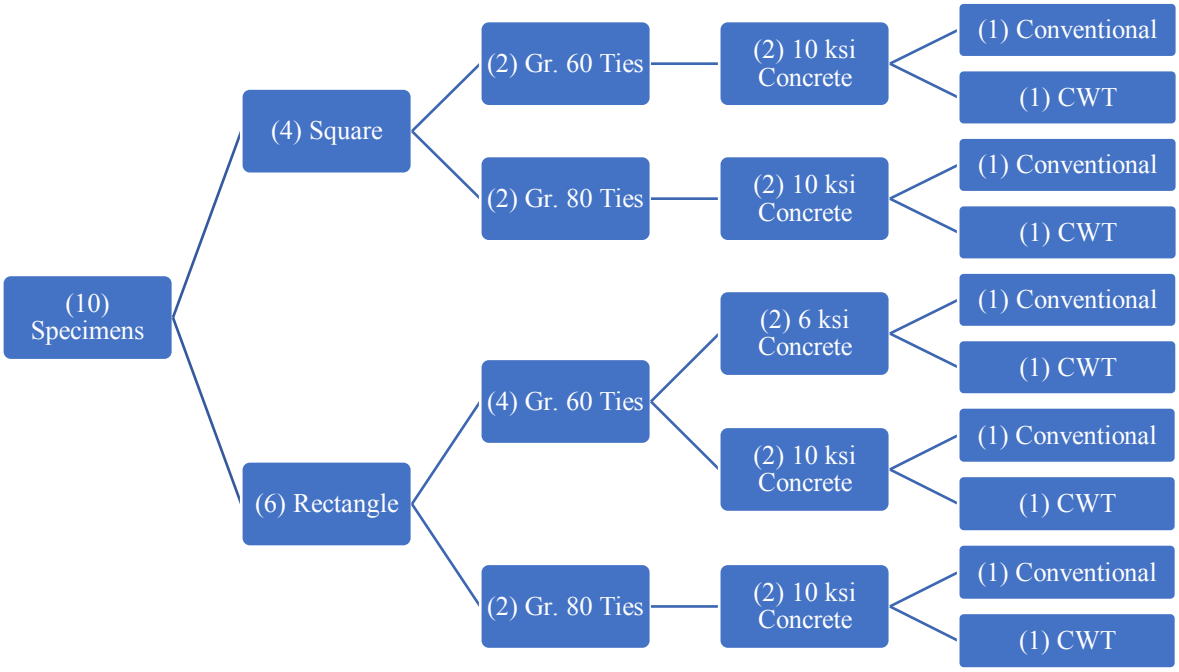

(a) Phase 1

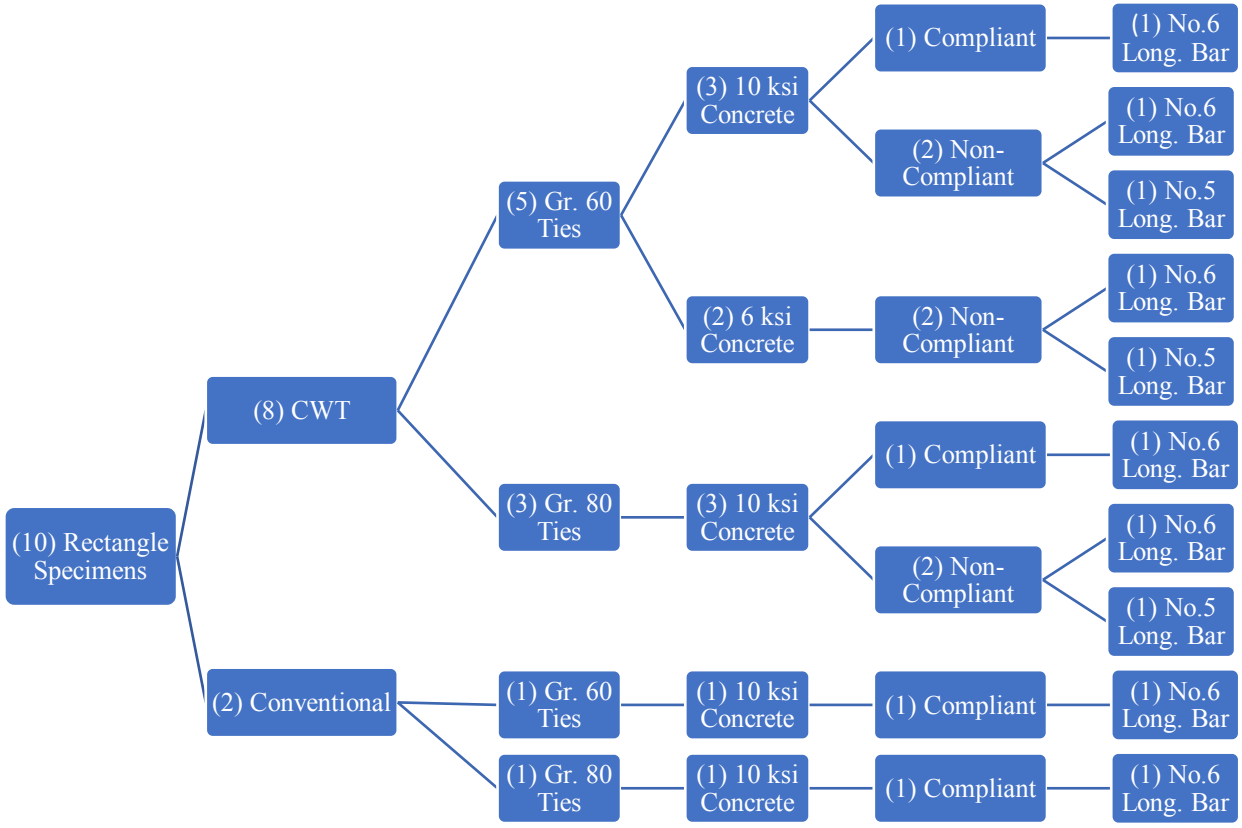

(b) Phase 2

Figure 2.1 Overview of test matrix

2.2 Test Specimens

The test specimens were designed as reduced scale SBEs based on the typical designs for high-rise special seismic wall construction provided by Dr. Reza Bayat. There was no specific prototype structure. High-rise core walls have a thickness between 24 in. and 36 in., with SBE length between 36 in. and 60 in. Longitudinal bars are typically No. 7 or No. 8 spaced around the perimeter of the wall at 6 in. on center, confined by No. 5 ties at 4 to 4 ½ in. on center. Concrete strength usually ranges from 8 to 10 ksi. Considering the testing machine capacity, a 0.6-scale factor was used to determine the dimensions, transverse bar sizes, longitudinal bar sizes, and longitudinal bar spacings of the test specimens. All the specimens were constructed at the University of Cincinnati and shipped to Richmond Field Station at the University of California-Berkeley.

2.2.1 Design methodology

For each specimen, the maximum expected axial load capacity was checked against the capacity of South Emery universal testing machine at the University of California-Berkeley Richmond Field Station, where the tests were conducted. The maximum usable machine capacity is 3900 kips. To determine the maximum expected axial capacity, the reduction factor for accidental eccentricity and strength reduction factor were neglected. Additionally, the nominal material strengths were increased by 20% and 25% for concrete and steel, respectively, to account for material overstrength and strength increase due to confinement effects.

2.2.2 Transverse and longitudinal reinforcement

One configuration of transverse and longitudinal reinforcement was used for the square specimens tested in Phase 1 (Figure 2.2). For the rectangular specimens, two configurations were utilized: (1) every other long-direction longitudinal bar was supported and (2) all the longitudinal bars in the long direction were supported, see Figure 2.2. Because of congestion issues, the same number of longitudinal bars could not be achieved for the second configuration. To maintain nearly equal longitudinal reinforcement ratios between the two configurations, fewer larger diameter reinforcing bars (12 No. 6) were used in the second configuration. The first configuration had a total of 18 No. 5 longitudinal reinforcing bars. Transverse reinforcement in all the specimens consisted of No. 4 hoops or CWTs. Noncompliance of six specimens in Phase 2 was achieved by assuming No. 5 hoops in design calculations but using No. 4 hoops in the test specimen. This approach allowed consistency throughout the noncompliant specimens and a realistic concept on how the ACI code could be altered.

2.2.3 Specimen details

Each specimen was a 6-ft tall stub column. This height was selected based on formwork and shipping considerations. A few measures were followed to attempt to induce failure in the central region. First, the ends were heavily reinforced with transverse ties at 2 in. spacing. Second, the central test region was made to be smaller in cross section than the ends. The central test region was detailed with no cover to focus on the core confined by CWTs or conventional ties in an effort to evaluate the effectiveness of the ties without the influence of the amount of concrete cover. With no clear cover, the only equation governing transverse steel volumetric ratio from Table 18.10.6.4(f) was Expression (b), previously defined as Eq. 1.2 in Chapter 1. Figure 2.3 illustrates a representative elevation for the 12 in. x 12 in. side of the specimens. To eliminate the need for hooks at the ends of the column longitudinal bars, the length of the heavily

confined ends was determined based on required development length of straight No. 5 bars in compression. Table 2.1 provides overall dimensions, transverse area reinforcement ratio (A_{sh}/sb_c), spacing (s/d_b ratios), and governing ACI 318-19 provision for the test specimens.

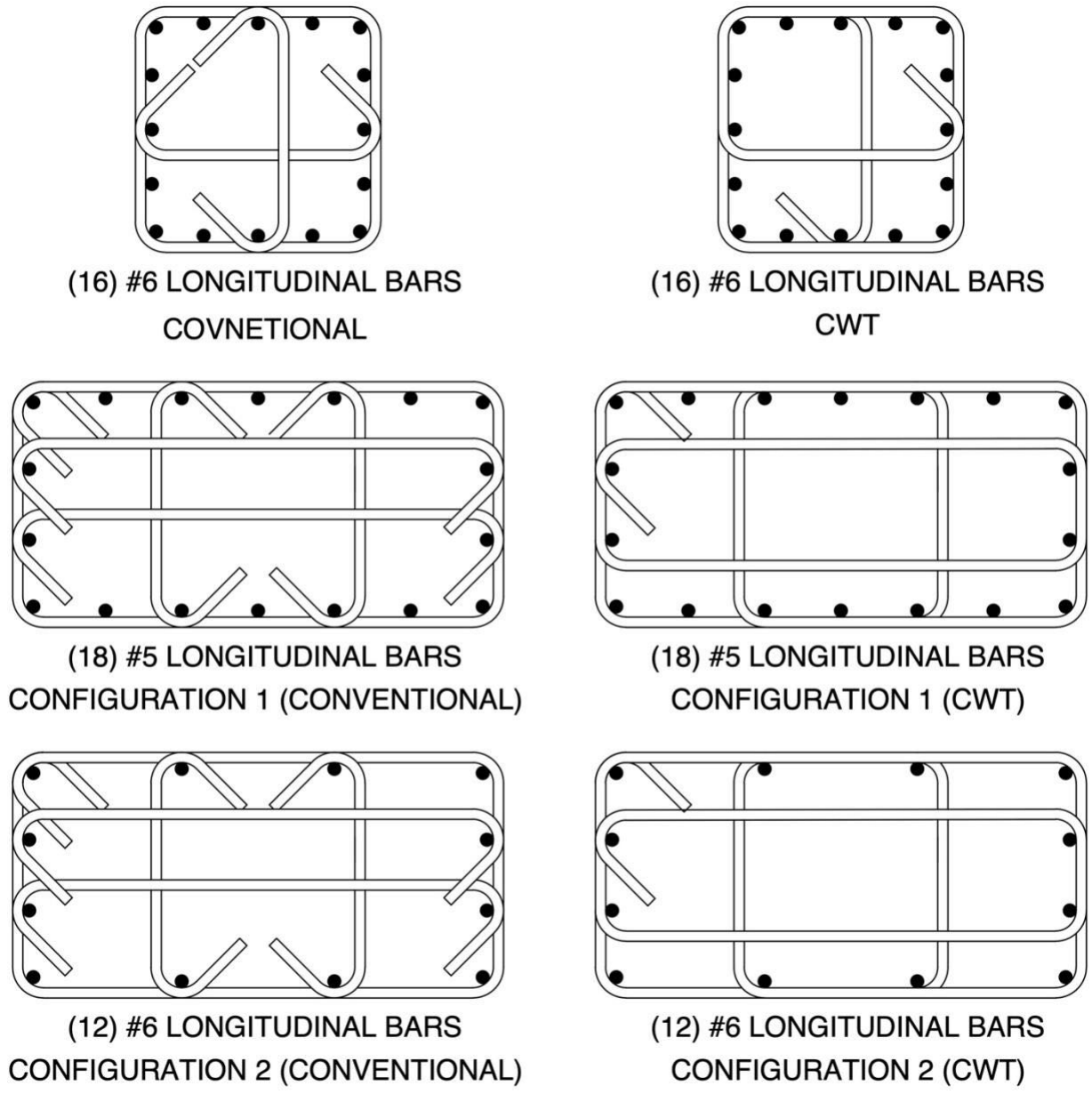

Figure 2.2 Configurations of longitudinal and transverse reinforcement

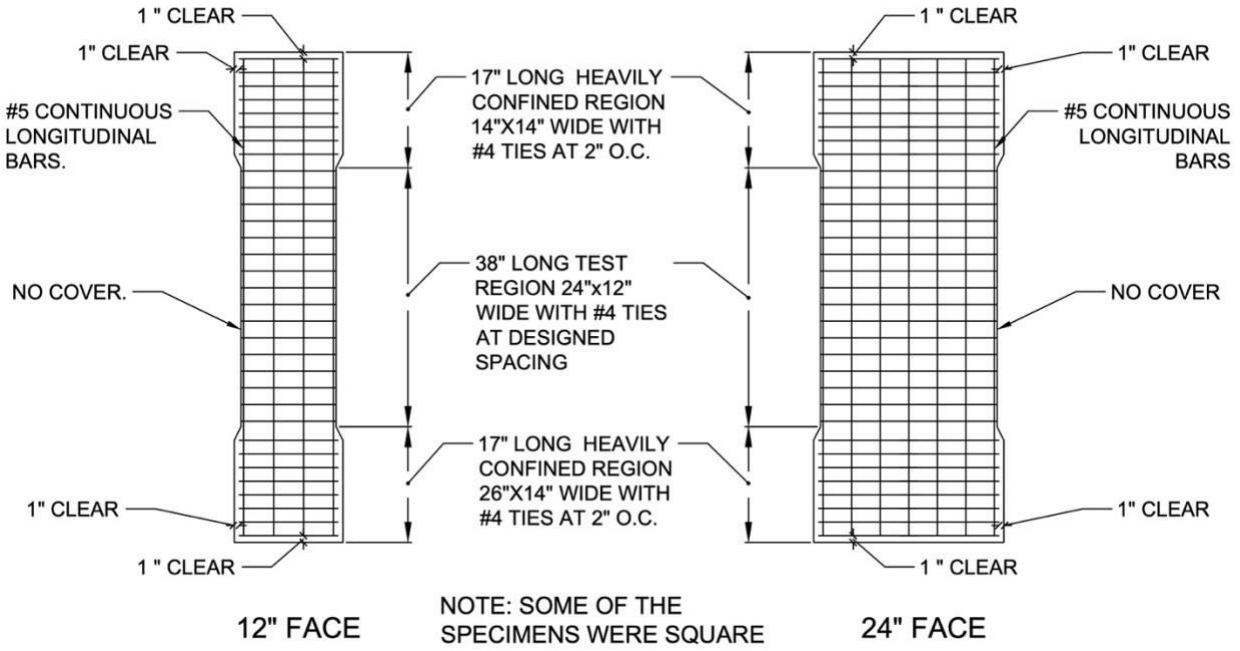

Figure 2.3 Representative specimen elevation view

Table 2.1 Test specimen details

Phase	Hoop Config.	Specimen ID	h (in.)	b (in.)	ρ	Req'd Tie Spacing (in.)	Min. A_{sh}/sb_c	Tie Vol. Ratio	s/d_b	Governing Code Provision	Actual Tie Spacing (in.)	Actual Outside Dimensions (in.)
1	1	CON-RT-Y-60-6-#5	24	12	0.0194	3.70	0.009	0.026	5.8	18.10.6.4	3-5/8	24-3/4 x 13-1/8
	1	CWT-RT-Y-60-6-#5	24	12	0.0194	3.70	0.009	0.030	5.8	18.10.6.4	3-5/8	24-3/4 x 13-1/8
	1	CON-RT-Y-60-10-#5	24	12	0.0194	2.22	0.016	0.044	3.4	18.10.6.4	2-1/8	24-3/4 x 13-1/8
	1	CWT-RT-Y-60-10-#5	24	12	0.0194	2.22	0.016	0.052	3.4	18.10.6.4	2-1/8	24-3/4 x 13-1/8
	1	CON-RT-Y-80-10-#5	24	12	0.0194	2.96	0.012	0.033	4.6	18.10.6.4	2-7/8	24-3/4 x 13-1/8
	1	CWT-RT-Y-80-10-#5	24	12	0.0194	2.96	0.012	0.038	4.6	18.10.6.4	2-7/8	24-3/4 x 13-1/8
	Square	CON-SQ-Y-60-10-#5	12	12	0.0344	3.33	0.015	0.028	5.2	18.10.6.4	3-1/4	13 x 13-1/8
	Square	CWT-SQ-Y-60-10-#5	12	12	0.0344	3.33	0.015	0.038	5.2	18.10.6.4	3-1/4	13 x 13-1/8
	Square	CON-SQ-Y-80-10-#5	12	12	0.0344	3.13	0.016	0.029	5.0	18.10.6.5b	3-1/8	13 x 13-1/8
	Square	CWT-SQ-Y-80-10-#5	12	12	0.0344	3.13	0.016	0.039	5.0	18.10.6.5b	3-1/8	13 x 13-1/8
2	2	CON-RT-Y-60-10-#6	24	12	0.0183	2.22	0.016	0.044	2.8	18.10.6.4	2-1/8	24-7/8 x 12-7/8
	2	CWT-RT-Y-60-10-#6	24	12	0.0183	2.22	0.016	0.052	2.8	18.10.6.4	2-1/8	25 x 13
	2	CON-RT-Y-80-10-#6	24	12	0.0183	2.96	0.012	0.033	3.8	18.10.6.4	2-7/8	25-1/4 x 13-1/4
	2	CWT-RT-Y-80-10-#6	24	12	0.0183	2.96	0.012	0.038	3.8	18.10.6.4	2-7/8	25 x 13
	1	CWT-RT-N-60-6-#5	24	12	0.0194	3.70	0.009	0.029	6.0	18.10.6.4	3-3/4	25 x 13-1/8
	1	CWT-RT-N-60-10-#5	24	12	0.0194	2.22	0.010	0.032	5.4	18.10.6.4	3-3/8	25 x 13
	1	CWT-RT-N-80-10-#5	24	12	0.0194	2.96	0.011	0.035	5.0	18.10.6.4	3-1/8	25 x 13
	2	CWT-RT-N-60-6-#6	24	12	0.0183	3.70	0.008	0.027	5.3	18.10.6.4	4-0	25 x 13
	2	CWT-RT-N-60-10-#6	24	12	0.0183	2.22	0.010	0.032	4.5	18.10.6.4	3-3/8	25 x 13
	2	CWT-RT-N-80-10-#6	24	12	0.0183	2.96	0.009	0.029	5.0	18.10.6.4	3-3/4	24-7/8 x 13-1/8

CON/CWT: conventional hoops/continuously wound ties; RT/SQ: rectangular square; Y/N: meets Code/does not meet Code; 60/80: Gr. 60/Gr. 80; 6/10: concrete strength in ksi; #5/#6: size of longitudinal bars

2.3 Fabrication

Reinforcing cages were tied at the University of Cincinnati Large Scale Test Facility by graduate students – see Figure 2.4. Insulation foam boards, shown in Figure 2.5, were used to achieve the reduced central test region for the specimens. During construction trials, it was discovered that, due to the tie wires and imperfect tie dimensions, the overall specimen

dimensions were slightly greater than the designed 12”x12” or 12”x24” dimensions measured from the outside of the hoops. Therefore, ½ in.-thick foam boards rather than 1 in.-thick foam boards were used to form the middle section to allow for dimensional imperfections. Even with minimal cover, ACI 318-19 Table 18.10.6.4(f) Expression (b), previously defined as Eq. 1.2 in Chapter 1, still governs tie spacing. The presence of some cover would only affect the axial compressive strengths. Before testing, the finished dimensions of the central test region were measured.

The specimens were cast upright (Figure 2.6). Around one hour after placing concrete, the tops of the specimens were covered with wet burlap and plastic sheathing to hold in moisture. Standard 6 in. x 12 in. test cylinders were made and cured next to the specimens in the same manner. The specimens and cylinders were wet cured for seven days.

(a) Tying of reinforcement cages

(b) Completed conventional cages

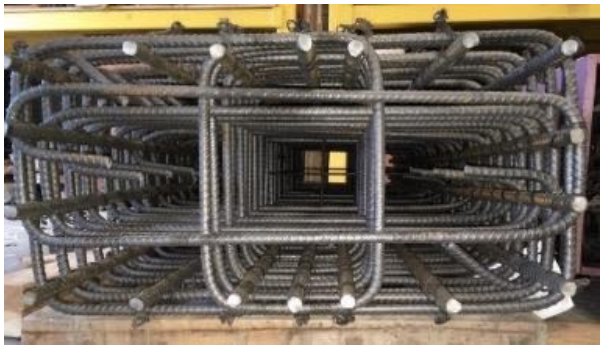

(c) Cross section of rectangular configuration 1 CWT specimen

(d) Cross section of rectangular configuration 2 CWT specimen

Figure 2.4 Reinforcement cages

Figure 2.5 Reinforcement cages wrapped in insulation foam boards

Figure 2.6 Formwork and curing

2.4 Test Setup, Protocol, and Instrumentation

The specimens were tested at Pacific Engineering Earthquake Research Center (PEER) at UC Berkeley under uniaxial, monotonically increasing compression utilizing the 4-million-lb-capacity (4000 kip) Southwark-Emery Testing Machine. The specimens were instrumented with LVDTs and strain gages on longitudinal and transverse reinforcement.

2.4.1 Instrumentation

The specimens were instrumented with displacement transducers (LVDTs) on all four faces of the specimen to measure the overall axial deformation, see Figure 2.7. Axial shortening was measured over approximately a 26-in. gage length. (The actual gage length was measured and used in data reduction.) Additionally, strains in the longitudinal bars and transverse reinforcement by strain gages. The locations of these gages are shown in Figure 2.8.

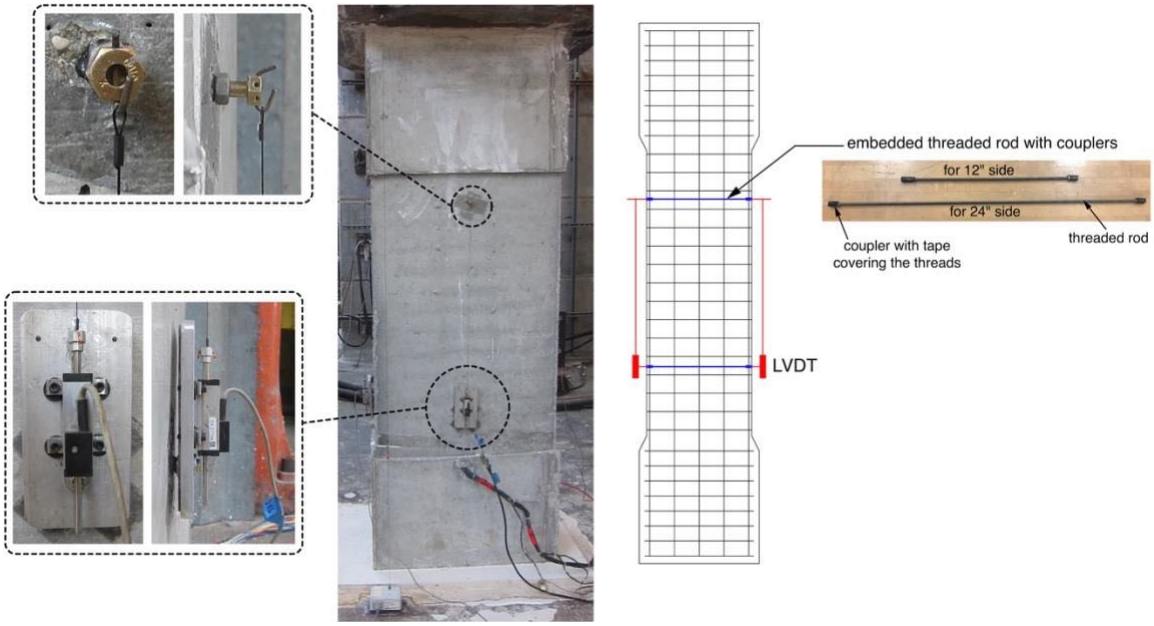

Figure 2.7 Measurement of axial shortening

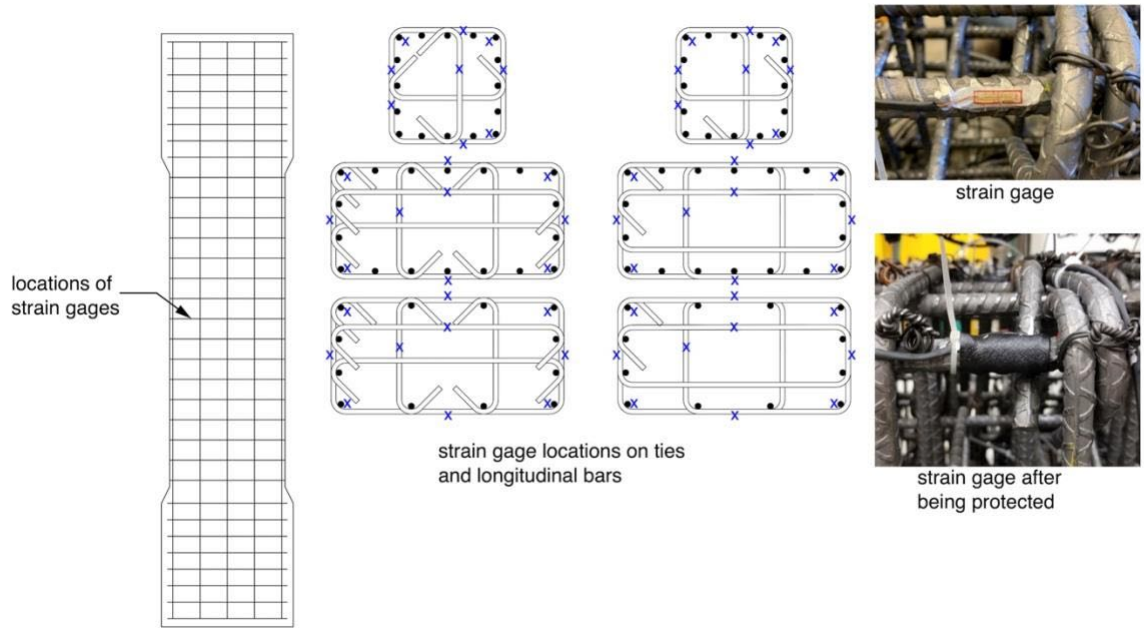

Figure 2.8 Strain gage locations

2.4.2 Test setup

The specimens were centered under the testing machine. After leveling and plumbing, the top and bottom faces were grouted with a thin layer of hydrostone (Figure 2.9). The hydrostone was allowed to cure for at least 20 hours before testing.

Figure 2.9 Bottom and top hydrostone layers

2.4.3 Test protocol

The specimens were loaded in concentric, monotonically increasing axial compression utilizing the 4-million-lb-capacity (4000 kips) Southwark-Emery Testing Machine (Figure 2.10). All specimens were initially tested under load-control mode. A target load rate of roughly 24,000 lb/min. was chosen for the tests to maintain a small strain rate. Testing of the first five Phase 1 specimens were stopped after specimen failure causing a sudden load drop. All the remaining specimens were tested until initial failure or load drop, and then testing continued in "acceleration-controlled mode" until the specimen was deemed unstable. The failures of the first five Phase 1 specimens were "explosive" in comparison to the failures of the remaining specimens. If possible, loading was continued in an attempt to capture post-peak behavior. Since the Southwark-Emery Testing Machine does not have a displacement control option, it was not possible to obtain extensive post-peak results for some of the specimens.

Figure 2.10 Overall view of test specimen

2.5 Material properties

The material properties for this project were measured with standard concrete cylinder compression tests and reinforcement tension tests.

2.5.1 Concrete

Hilltop Basic Resources in Cincinnati developed the concrete mix designs for both the 6000 psi and 10000 psi concrete mixes. A summary of the concrete mix designs is provided in Table 2.2. Standard 6 in. x 12 in. cylinders were site-cured with the same conditions as the specimens to obtain a better measure of compressive strengths considering site conditions. For Phase 1 and Phase 2, site-cured cylinders were placed next to the test specimens. In Phase 2, additional cylinders were placed in an area with more shade but still close to the test specimens. Due to the nature of site-cured cylinders, the compressive strengths are lower than they would be if they were cured per ASTM C31. The measured compressive strengths are summarized in Table 2.3.

Table 2.2 Concrete mix designs

Mix	**6000 psi**	**10000 psi**
Materials	**Qty**	**Qty**
Portland Cement (lbs/cy)	500	555
GRAN-CEM (lbs/cy)	-	295
Fine Aggregate (lbs/cy)	1328	1073
Mid-size Aggregate (lbs/cy)	-	400
Coarse Aggregate (lbs/cy)	1850	1400
Water (lbs/cy)	260	295
Fly Ash (lbs/cy)	100	-
Glenium 7500 (oz/cy)	24	51
Water Reducer Std.	-	34
WR ASTM C494 Type A, B, & C (oz/cy)	24	-
w/c ratio	0.43	0.35
Unit Weight (lbs/cy)	149.5	148.8
Slump (in.)	8	8
Air Content (%)	1.5	1.5

Table 2.3 Summary of compressive strengths

Phase	Age (days)	6000 psi mix	10000 psi mix
1	10	5010	7700
	28	6610	8710
	47	6380	----
	49	6830	----
	54	----	8750
	60	----	9400
	63	----	8640
2	7	4760	8190
	28	5400	9380
	33	5190	9400
	57	5350	9400

2.5.2 Reinforcement

Due to the fabrication challenges encountered in this project, four suppliers provided the reinforcement for Phase 1. All the reinforcement for Phase 2 was provided by one supplier. The measured material properties are shown in Table 2.4.

Table 2.4 Reinforcement measured material properties

Phase	Size	Grade	Source	f_y (ksi)	f_u (ksi)	Elongation (%)
1	No. 4	A706 Gr. 60	1	63.7	87	15.7
	No. 4	A706 Gr. 60	2	62.5	92.7	10.6
	No. 4	A706 Gr. 80	2	89.7	122	8.90
	No. 4	A706 Gr. 80	3	79.1	113	7.63
	No. 5	A706 Gr. 60	1	67.7	92.4	9.93
	No. 5	A706 Gr. 80	4	86.9	114	8.47
2	No. 4	A706 Gr. 60	5	70.6	97.6	21.6
	No. 4	A706 Gr. 80	5	85.3	118	8.32
	No. 5	A706 Gr. 60	5	66.8	95.1	19.0
	No. 5	A706 Gr. 80	5	82.1	107	16.5
	No. 6	A706 Gr. 60	5	70.7	96.4	19.1
	No. 6	A706 Gr. 80	5	84.3	111	15.6

Chapter 3 Test Results and Discussions

3.1 Introduction

An overview of the specimens is provided based on visual descriptions of the damage patterns and failed specimens. The measured data are synthesized in an effort to compare the performance of conventional transverse reinforcement and continuously wound ties (CWTs).

3.2 Damage and Failure Patterns

A visual description of each failed specimen is provided, including the general location of the main failure indicated by concrete core crushing, location and description of longitudinal bar buckling and/or fractures, and the location and description of transverse reinforcement deformations and/or fractures. The elevation photos of each face of the specimen were taken before any loose concrete was removed after tests were concluded. After initial photos were taken, loose concrete was removed allowing for further inspection of the reinforcement and damage zone.

3.2.1 Specimen CON-RT-Y-60-#5

Different views of the damage are shown in Figure 3.1. The west face of the specimen failed primarily in the bottom half of the central test region, while the east face failed primarily in the top half of the central test region. The north and south faces failed at center height of the specimen. Longitudinal bars buckled and transverse reinforcement deformed outward in the damaged regions. Supported bars appeared to have buckled over one bar length (defined as the length between two consecutive transverse reinforcement), while laterally unsupported bars appeared to have buckled over two bar lengths (defined as the length between three consecutive transverse reinforcement). A total of 16/18 (89%) of the longitudinal bars buckled. A 135-degree hook around an interior longitudinal bar straightened on the east face. See Figure 3.1e for buckled longitudinal reinforcement and bulged ties on the east face of the specimen.

(a) west face

(b) north and east faces

(c) east face

(d) south and east faces

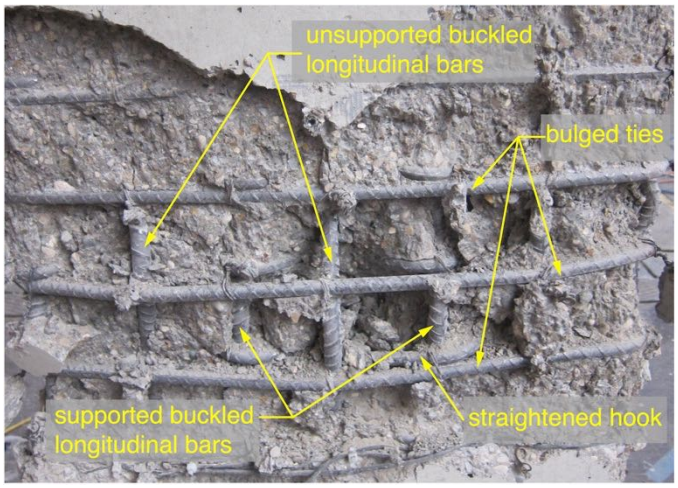

(e) buckled and deformed reinforcement on east face

Figure 3.1 Damage patterns for specimen CON-RT-Y-60-#5

3.2.2 Specimen CWT-RT-Y-60-6-#5

The west face of the specimen was primarily damaged near center height of the specimen (Figure 3.2a). On the west face, all the longitudinal bars buckled over one bar length (Figure 3.2e). However, the buckled portion of the unsupported longitudinal bars adjacent to the corner bars bulged outward more than the other longitudinal bars. The instrumented center tie was deformed outward. The north and south faces of the specimen (Figure 3.2b and Figure 3.2d, respectively) were damaged near the center of the central test region, but there were no significant tie deformations, and only one interior bar slightly buckled on each face. The east face (Figure 3.2c) was damaged at the bottom of the central test region. The second tie from the bottom of the central test region was significantly deformed outward, and the unsupported bars adjacent to the corner bars buckled. The center unsupported longitudinal bar, north corner bar, and supported longitudinal bar to the south of the center only slightly buckled, and the remaining longitudinal bars on the east face did not buckle. In summary, 14/18 (78%) of the longitudinal bars showed some degree of buckling, and all buckled longitudinal bars generally buckled over one bar length.

(a) west face

(b) north and east faces

(c) east face

(d) south and east faces

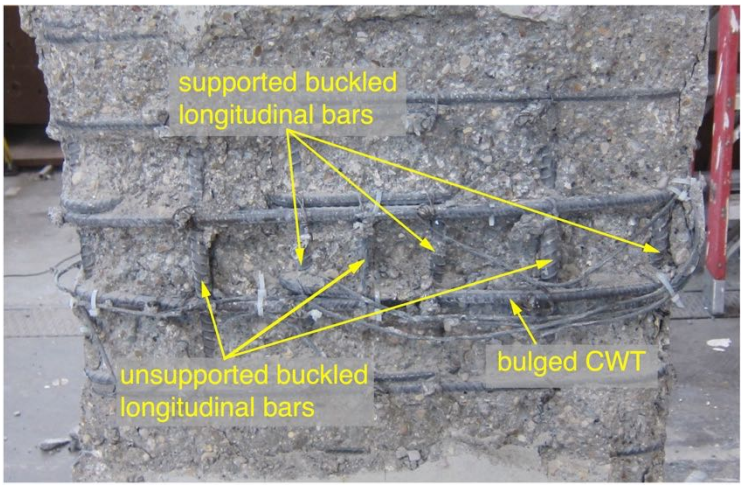

(e) buckled and deformed reinforcement on east face

Figure 3.2 Damage patterns for specimen CWT-RT-Y-60-6-#5

3.2.3 Specimen CON-RT-Y-60-10-#5

There was no significant damage on the west face of the specimen (Figure 3.3a) in the central test region, though there was some spalling at the top and bottom of heavily confined end regions of the specimen. There was no significant longitudinal bar buckling or tie deformations on the north or south faces (Figure 3.3b and Figure 3.3d, respectively). The north face exhibited some damage in the concrete core towards the east side of the specimen in the central test region. The south side underwent some damage, primarily in the bottom east half of the central test region. The east face was damaged throughout most of the central test region (Figure 3.3c). The most severe core crushing occurred within the middle 16 in. of the central test region. At the center height of the specimen, the laterally unsupported bars directly adjacent to the corner bars buckled over approximately 2 bar lengths. The middle laterally unsupported longitudinal bar buckled over three bar lengths (Figure 3.3e). The remaining longitudinal bars did not buckle. Two ties near the middle longitudinal bar were deformed outward, and a 135-degree hook was straightened. In total, 3/18 (17%) of the longitudinal bars buckled, all on the east face.

(a) west face

(b) north and east faces

(c) east face

(d) south and east faces

(e) east face buckled middle longitudinal bar

Figure 3.3 Damage patterns for specimen CON-RT-Y-60-10-#5

3.2.4 Specimen CWT-RT-Y-60-10-#5

The west face was primarily damaged over the bottom half of the central test region (Figure 3.4a). The unsupported middle longitudinal bar and longitudinal bars adjacent to the corner longitudinal bars as well as the supported longitudinal bar to the east of center buckled over two bar lengths. Two CWTs were deformed outward near the buckled longitudinal bars, and a CWT leg ruptured at the longitudinal bar to the north of the center bar (Figure 3.4e). Damage was observed throughout the central test region on north and south faces (Figure 3.4b and Figure 3.4d, respectively). However, there were no observed tie or longitudinal bar deformations, except on the south face on which the east corner longitudinal bar buckled over one bar length. The east face was primarily damaged just above the center of the specimen (Figure 3.4c). The three ties above the center instrumented tie were deformed outward. The two laterally unsupported longitudinal bars adjacent to the corner bars buckled over two bar lengths. The center bar and the laterally supported bar south of the center bar buckled over one bar length, see Figure 3.4f. In total, 9/19 (50%) of the longitudinal bars buckled one to two bar lengths.

(a) west face

(b) north and east faces

(c) east face

(d) south and east faces

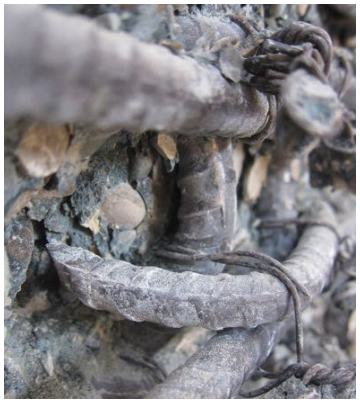

(e) west face ruptured CWT leg at the first bar north of the center bar

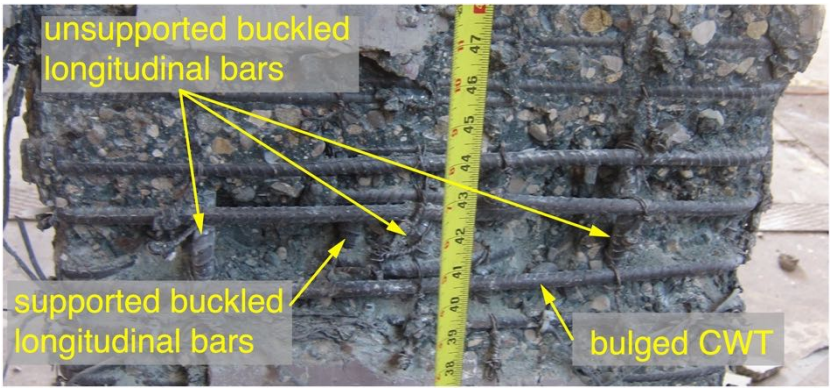

(f) buckled and deformed reinforcement on east face

Figure 3.4 Damage patterns for specimen CWT-RT-Y-60-10-#5

3.2.5 Specimen CON-RT-Y-80-10-#5

Damage on the west face was concentrated to the bottom 28 in. of the specimen (Figure 3.5a). Some small outward tie deformations and minimal core crushing were observed. The northwest corner longitudinal bar buckled one bar length 20 in. from the bottom of the specimen. The north face was damaged, including some core crushing, in the bottom half of the central test region (Figure 3.5b). The south face was damaged with some core crushing in the central test region primarily on the south side (Figure 3.5d). Neither the north nor the south face had evidence of longitudinal bar buckling or notable tie deformations. Concrete was damaged throughout most of the central test region on the east face (Figure 3.5c), with primary core damage, longitudinal bar buckling, and outward tie deformations occurring within the center 16 in. of the central test region. The longitudinal bars on the south side buckled below mid-height of the specimen, while the middle longitudinal bar and longitudinal bars on the north side buckled above mid-height of the specimen (Figure 3.5e). The laterally unsupported longitudinal bars adjacent to the corner bars buckled over two bar lengths. The laterally supported longitudinal bars adjacent to the middle bar buckled over one bar length. The middle laterally

unsupported longitudinal bar buckled over three bar lengths. In general, 6/18 (33%) of the longitudinal bars buckled, with the majority of buckled bars being located on the east face.

(a) west face

(b) north and west faces

(c) east face

(d) south and east faces

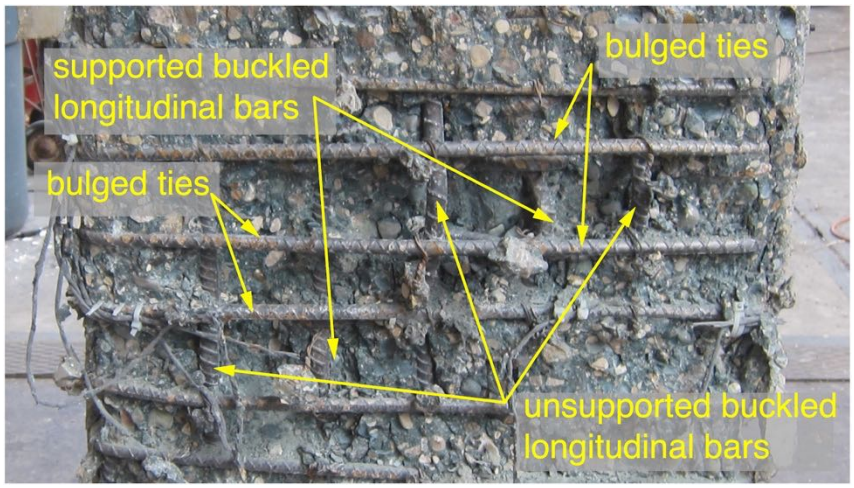

(e) east face buckled middle longitudinal bar

Figure 3.5 Damage patterns for specimen CON-RT-Y-80-10-#5

3.2.6 Specimen CWT-RT-Y-80-10-#5

In general, there was extensive core damage in the primary failure regions. Every longitudinal bar in the core damage region buckled over two to four bar lengths, often forming "S" shapes and buckling in multiple planes. The west face damage was concentrated over the bottom 10 in. of the central test region (Figure 3.6a). Damage consisted of outward deformed ties and buckled longitudinal bars (Figure 3.6e). The two laterally supported longitudinal bars adjacent to the center bar and the corner bars fractured. Hooks were straightened at the north corner longitudinal bar. The damaged regions and ties on the north and south faces (Figure 3.6b and Figure 3.6d, respectively) sloped down from the east to west. Both laterally supported interior longitudinal bars fractured on each face. On the south face, two CWTs fractured, one of them with two fractured legs. On the north face, one CWT was fractured in two locations. The east face was primarily damaged in a region 38 in. to 47 in. above the bottom of the specimen (Figure 3.6c and Figure 3.6f). A CWT was fractured in two locations near the center

longitudinal bar. At the south corner longitudinal bar, a CWT leg was fractured, and two 135-degree hooks were straightened. Additionally, the second longitudinal bar from the north face was fractured. In general, five longitudinal bars were fractured, transverse reinforcement legs were fractured at nine locations, and 135-degree hooks were straightened at 3/12 (25%) of the supported longitudinal bars.

(a) west face

(b) north and west faces

(c) east face

(d) south and east faces

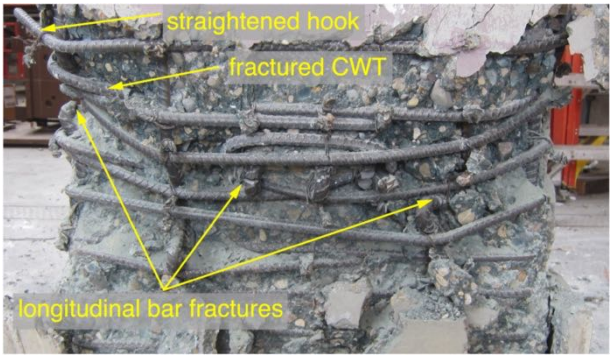

(e) damaged region on west face

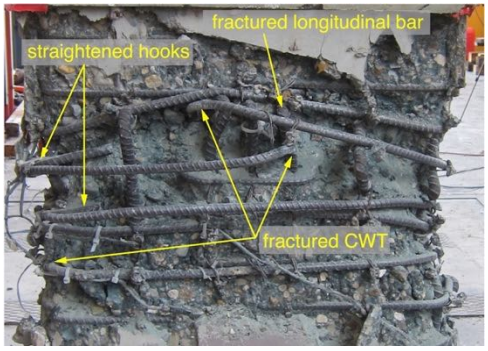

(f) damaged region on east face

Figure 3.6 Damage patterns for specimen CWT-RT-Y-80-10-#5

3.2.7 Specimen CON-SQ-Y-60-10-#5

The most severe concrete core damage was concentrated in the bottom 12 in. of the specimen in the heavily confined end region. Every longitudinal bar in the damaged region buckled in "S" shapes over three to four bar lengths and sometimes in multiple planes, and the hoops in the damaged regions deformed outward. Some cover spalled in the bottom of the central test region on the west (Figure 3.7a) and south (Figure 3.7d) faces of the specimen, but the east (Figure 3.7c) and north (Figure 3.7b) faces in the central test region had minimal spalling. Two 135-degree hooks straightened at the south-west and north-east corner longitudinal bars (Figure 3.7e). Most of the 135-degree hooks supporting the center longitudinal bar near the buckled location straightened, and hooks also straightened at three out of the four corner longitudinal bars. On the east face, two outer hoops and the hook supporting the center longitudinal bar fractured (Figure 3.7f). In summary, no longitudinal bars fractured, three tie

legs fractured, and 135-degree hooks straightened at 7/8 (88%) of the supported longitudinal bars.

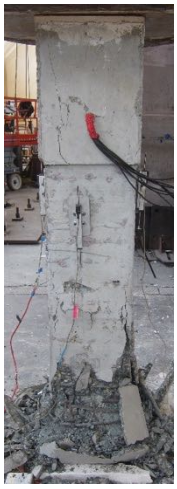

(a) west face

(b) north and west faces

(c) east face

(d) south and east faces

(e) straightened 135-degree seismic hooks at the north-east corner longitudinal bar

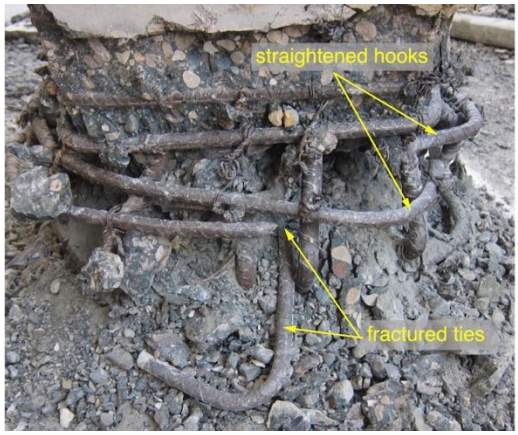

(f) fractured hoop and tie leg on the east face

Figure 3.7 Damage patterns for specimen CON-SQ-Y-60-10-#5

3.2.8 Specimen CWT-SQ-Y-60-10-#5

In general, there was extensive core damage near mid-height of the central test region. In the damaged regions, every longitudinal bar buckled over two to four bar lengths, often in "S" shapes and in multiple planes, and ties deformed outward. See Figure 3.8a, Figure 3.8b, Figure 3.8c, and Figure 3.8d for elevations of the west, north, east, and south faces of the specimen, respectively. A CWT outer leg on both the west and south faces fractured. A CWT also fractured at the south-east corner longitudinal bar. Additionally, at the center longitudinal bar on the north face, an outer leg and a tie leg of one CWT fractured (Figure 3.8e). In summary, no longitudinal bars fractured, transverse tie legs fractured in five locations, and none of the 135-degree hooks at the eight supported longitudinal bars were straightened.

(a) west face

(b) north and west faces

(c) east face

(d) south and east faces

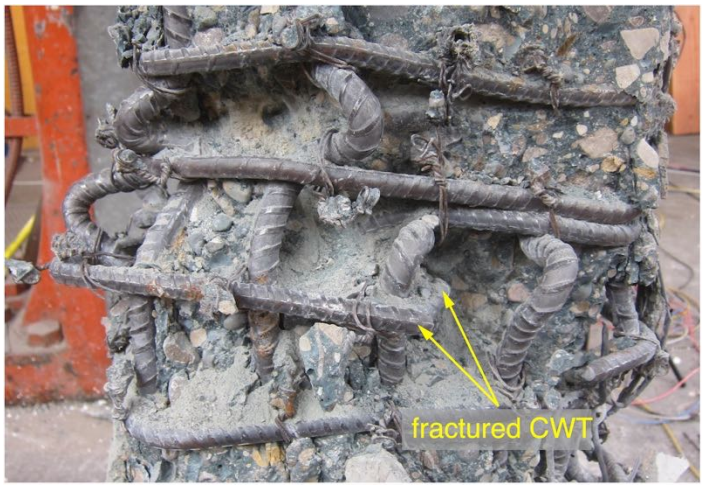

(e) damage and transvese reinforcement fracture on north face

Figure 3.8 Damage patterns for specimen CWT-SQ-Y-60-10-#5

3.2.9 Specimen CON-SQ-Y-80-10-#5

In general, there was extensive concrete core damage near mid-height of the central test region and much of the concrete spalled throughout the central test region. In the damaged regions, every longitudinal bar buckled over two to four bar lengths, often in "S" shapes and in multiple planes, and ties deformed outward. See Figure 3.9a, Figure 3.9b, Figure 3.9c, and Figure 3.9d for elevation views of the west, north, east, and south faces of the specimen, respectively. A 135-degree hook straightened in the damaged region at both the north-west and south-east corner longitudinal bars (Figure 3.9e). Additionally, 135-degree hook supporting the center buckled longitudinal bar straightened to some extent on each face of the specimen (Figure 3.9f) and a tie fractured on the south face. In summary, no longitudinal bars fractured, one tie leg fractured, and 135-degree hooks straightened at 6/8 (75%) of the supported longitudinal bars.

(a) west face

(b) north and east faces

(c) east face

(d) south faces

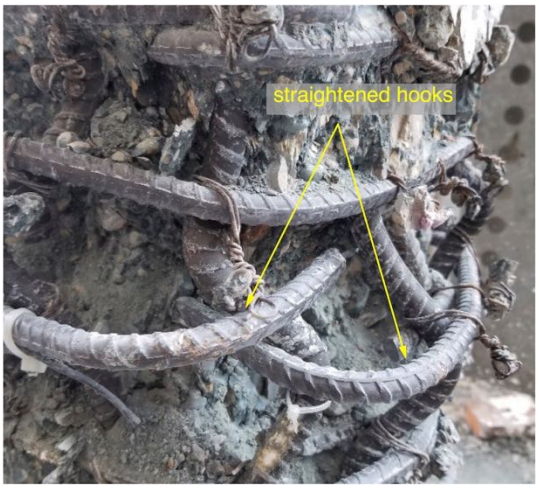

(e) 135-degree hooks straightening and pulling out at the south-east corner longitudinal bar

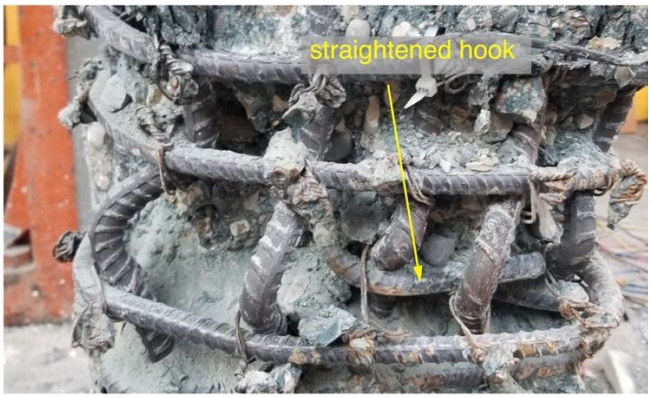

(f) 135-degree hook straightening at the middle longitudinal bar on the south face

Figure 3.9 Damage patterns for specimen CON-SQ-Y-80-10-#5

3.2.10 Specimen CWT-SQ-Y-80-10-#5

Most of the core damage was concentrated in the bottom heavily confined end region and the bottom of the central test region. The cover on west (Figure 3.10a) and north (Figure 3.10b) faces spalled over most of the specimen face. On the east (Figure 3.10c) and south (Figure 3.10d) faces, cover spalled primarily towards the bottom of the specimen and corners. Most core damage on the west and south faces occurred 21 in. from the bottom of the specimen (about 6 in. into the central test region) and below, while most core damage on the north and east faces occurred within the bottom 10 in. of the specimen. In the core damaged regions, every longitudinal bar buckled over two to five bar lengths and ties were deformed outward where the longitudinal bars buckled. The following transverse reinforcement fractures were found: one tie on the west and north faces, two ties on the south face, and three ties on the east face (Figure 3.10e). A tie fractured at both the south-east and north-west corners. In summary, no longitudinal bars fractured, transverse reinforcement fractured at nine locations, and a 135-degree hook straightened at one of the supported longitudinal bars.

(a) west face

(b) north and west faces

(c) east face

(d) south and east faces

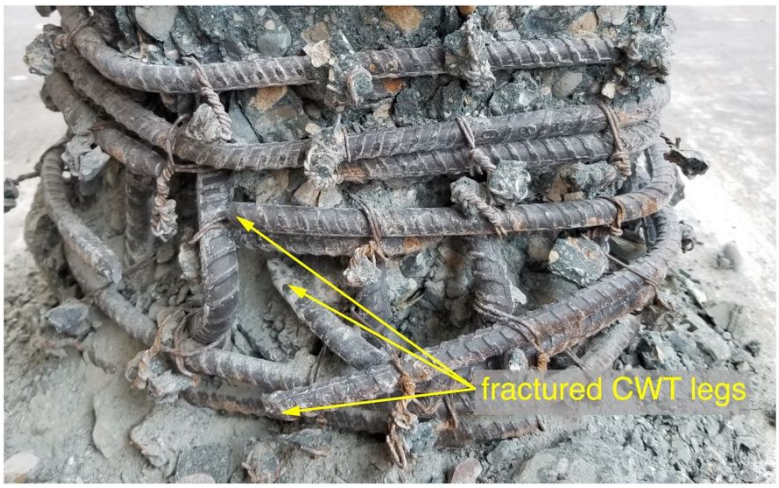

(e) east face damage

Figure 3.10 Damage patterns for specimen CWT-SQ-Y-80-10-#5

3.2.11 Specimen CON-RT-Y-60-10-#6

Most of the core damage was concentrated on the west face of the central test region. The cover on west face (Figure 3.11a) spalled over most of the specimen face. On the east (Figure 3.11c) and south (Figure 3.11d) faces, cover spalled primarily towards the bottom of the specimen and corners. Two supported longitudinal bars on the west face buckled over one bar length (defined as the length between two consecutive transverse reinforcement) within the bottom quarter of the test region (Figure 3.11e and Figure 3.11f). No longitudinal bar or transverse reinforcement fractured. None of the hooks straightened.

(a) west face

(b) north and west faces

(c) east face

(d) east and south faces

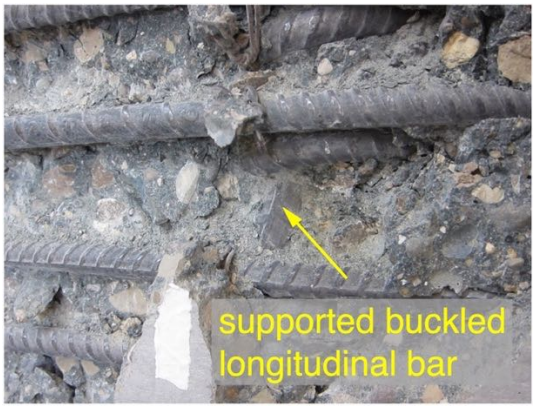

(e) west face damage

(f) south face damage

Figure 3.11 Damage patterns for specimen CON-RT-Y-60-10-#6

3.2.12 Specimen CWT-RT-Y-60-10-#6

Most of the core damage was concentrated on the west face of the central test region (Figure 3.12). The cover on west face spalled over the bottom half of the specimen face. Four supported longitudinal bars (out of twelve bars) buckled on the west face near the middle of the test region. The buckling length was one bar length, which is defined as the length between two consecutive transverse reinforcement. No longitudinal bar or transverse reinforcement fractured. None of the hooks straightened.

(a) west face

(b) north and west faces

(c) east face

(d) south and east faces

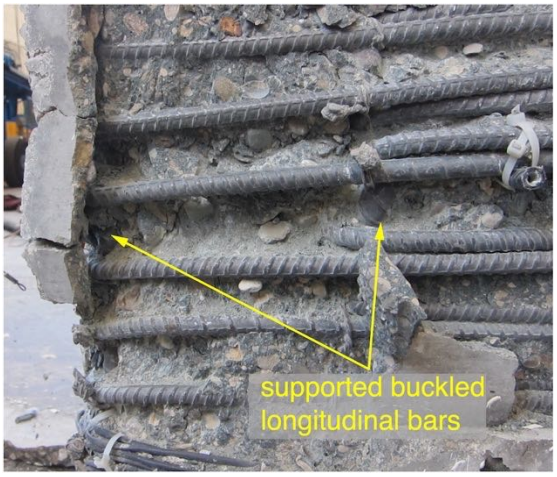

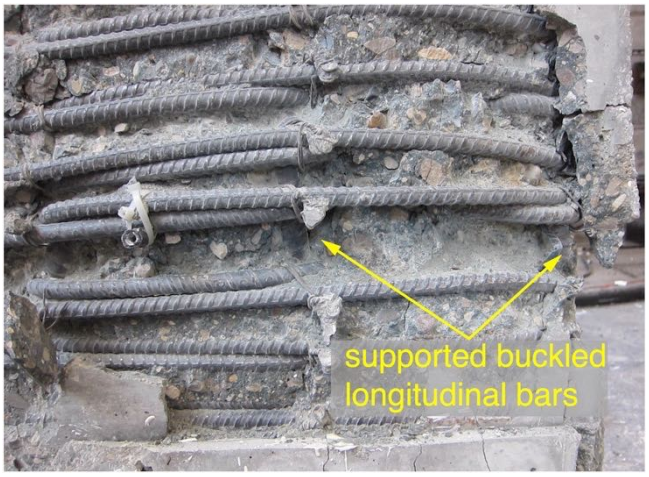

(e) west face damage

Figure 3.12 Damage patterns for specimen CWT-RT-Y-60-10-#6

3.2.13 Specimen CON-RT-Y-80-10-#6

Damage was distributed among all four faces (Figure 3.13). The damage on the west side was towards the top whereas it was near the bottom on the east face. Four and three supported longitudinal bars buckled on the west face and east face, respectively. Therefore, 58% (7 out of 12) of the longitudinal bars buckled. One transverse reinforcement (CON) was fractured on the north face. One supported longitudinal bar also buckled on the north face. None of the hooks straightened

(a) west face

(b) north and west faces

(c) east face

(d) south and east faces

(e) damage on west face

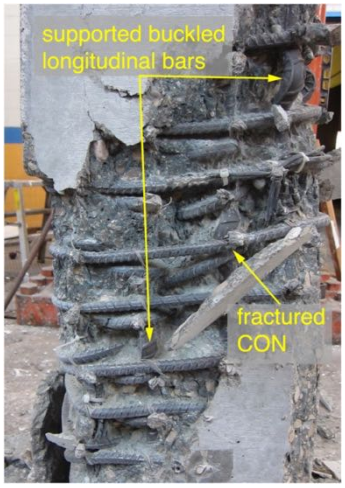

(f) damage on north face

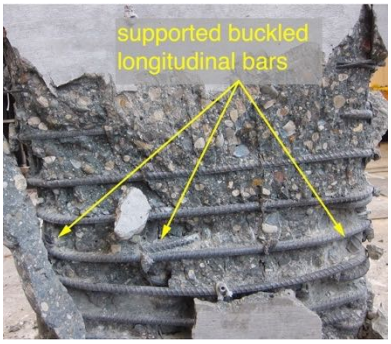

(g) damage on east face

Figure 3.13 Damage patterns for specimen CON-RT-Y-80-10-#6

3.2.14 Specimen CWT-RT-Y-80-10-#6

As seen from Figure 3.14, all four faces experienced damage over the test region. All four supported corner longitudinal bars buckled. In addition, two supported intermediate longitudinal bars on the east and south face buckled. The tie on the south was pushed outward due to the buckling of one of the longitudinal bars. One tie was found to have straightened on the east face. One supported longitudinal bar on the north face buckled. For all the buckled bars, buckling occurred over one bar length (defined as the length between two consecutive transverse reinforcement).

(a) west face

(b) south and west faces

(c) east face

(d) north and east faces

(e) damage on west face

(f) damage on south face

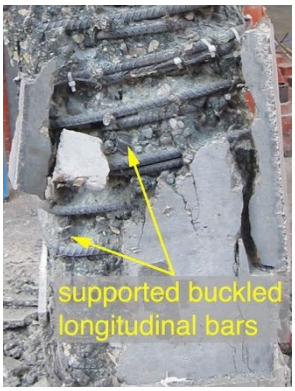

(g) damage on north face

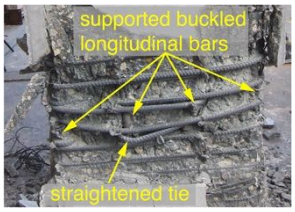

(h) damage on east face

Figure 3.14 Damage patterns for specimen CWT-RT-Y-80-10-#6

3.2.15 Specimen CWT-RT-N-60-6-#5

All the supported and unsupported longitudinal bars buckled on all faces over one bar length, see Figure 3.15. None of the reinforcement fractured.

(a) west face

(b) north and west faces

(c) east face

(d) south and east faces

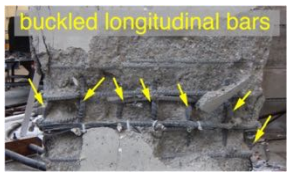

(e) damage on west face

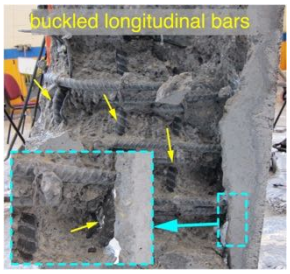

(f) damage on south face

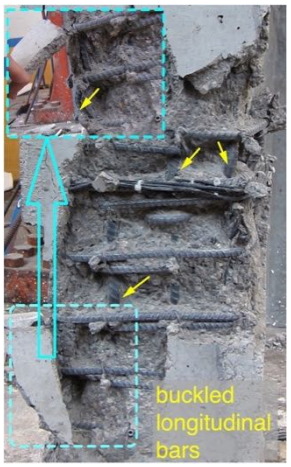

(g) damage on north face

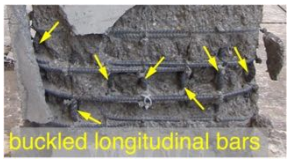

(h) damage on east face

Figure 3.15 Damage patterns for specimen CWT-RT-N-60-6-#5

3.2.16 Specimen CWT-RT-N-60-10-#5

Supported corner bars and unsupported intermediate longitudinal bars buckled on the west and east faces. The buckled corner bars are also visible from the south and north faces, see Figure 3.16. The bars buckled between two consecutive transverse reinforcement, i.e., over one bar length.

(a) west face

(b) north and west faces

(c) east face

(d) south and east faces

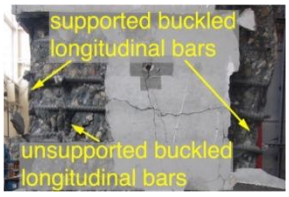

(e) damage on west face

(f) damage on south face

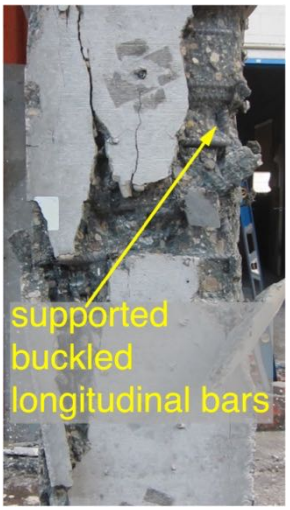

(g) damage on north face

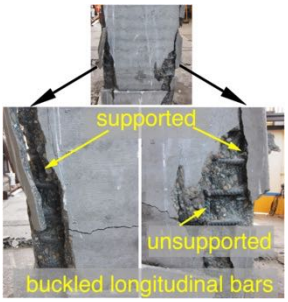

(h) damage on east face

Figure 3.16 Damage patterns for specimen CWT-RT-N-60-10-#5

3.2.17 Specimen CWT-RT-N-80-10-#5

All the longitudinal bars (supported or not supported) buckled on the east and west faces, which were the long side. On the north and south faces, three supported longitudinal bars buckled. The corner bar on the south bar buckled over three bar lengths (defined as the length between four consecutive transverse reinforcement). One leg of CWT fractured on the south face. The damage patterns are shown in Figure 3.17, which shows all faces were damaged.

(a) west face

(b) north and west faces

(c) east face

(d) south and east faces

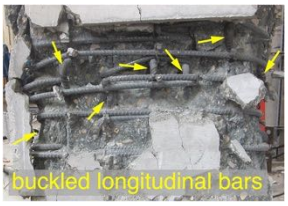

(e) damage on west face

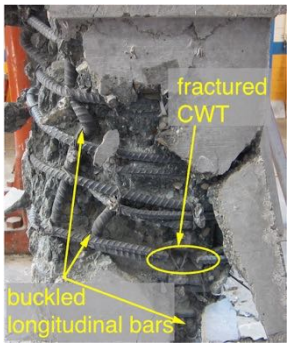

(f) damage on south face

(g) damage on north face

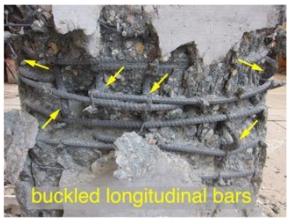

(h) damage on east face

Figure 3.17 Damage patterns for specimen CWT-RT-N-80-10-#5

3.2.18 Specimen CWT-RT-N-60-6-#6

In this specimen, the damage was concentrated on north, south, and west faces – see Figure 3.18. On all these faces, all the longitudinal bars were supported and buckled. The damage on the east face was full separation of cover from the core. The reinforcement (longitudinal and transverse) did not rupture.

(a) west face

(b) north and west faces

(c) east face

(d) south and east faces

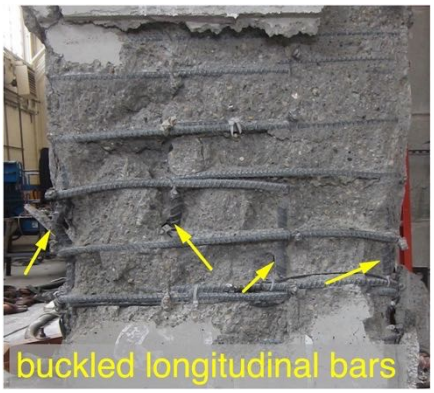

(e) damage on west face

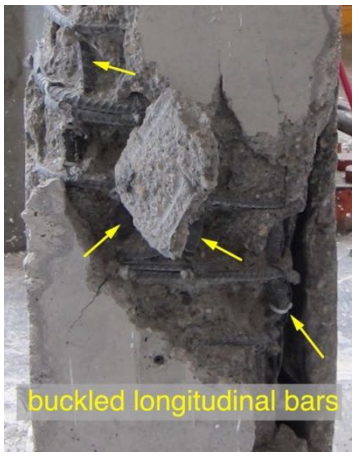

(f) damage on south face

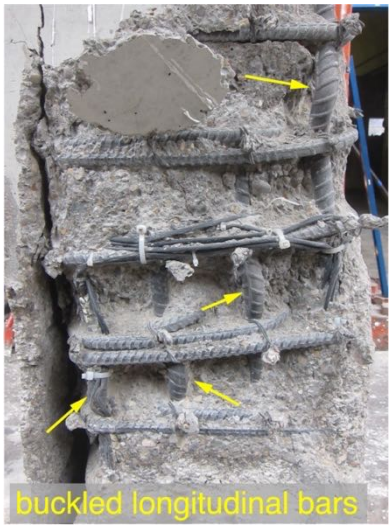

(g) damage on north face

Figure 3.18 Damage patterns for specimen CWT-RT-N-60-6-#6

3.2.19 Specimen CWT-RT-N-60-6-#6

As seen from Figure 3.19, the east face experienced minor damage consisting of delamination of a part of the cover. On the other hand, significant damage occurred in the other three faces. All the longitudinal bars, which were supported, buckled on the west and north faces. A corner bar on the north face buckled over three lengths (defined as the length between four consecutive transverse reinforcement).

(a) west face

(b) north and west faces

(c) east face

(d) south and east faces

(e) damage on west face

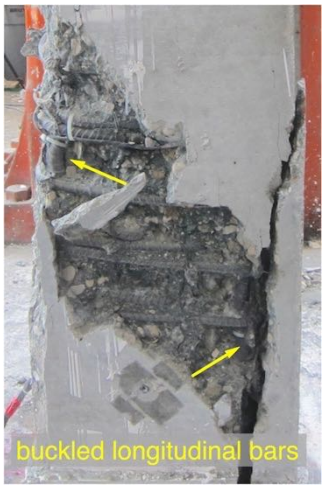

(f) damage on south face

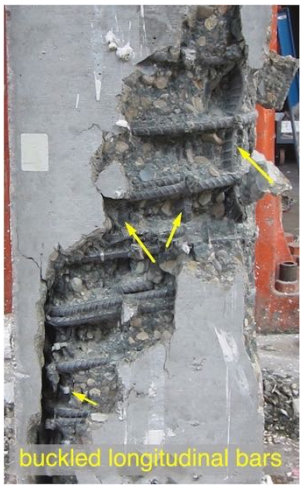

(g) damage on north face

Figure 3.19 Damage patterns for specimen CWT-RT-N-60-6-#6

3.2.20 Specimen CWT-RT-N-80-10-#6

All faces were damaged (Figure 3.20). Buckling of longitudinal bars, which were all supported, occurred with differing degrees on all faces. On the south and east faces, three longitudinal bars buckled. Two buckled longitudinal bars could be identified on the west face. Four longitudinal bars buckled on the north face, one of the corner bars buckled over two bar lengths (defined as the length between three consecutive transverse reinforcement). The longitudinal or transverse reinforcement did not fracture.

(a) west face

(b) north and west face

(c) east face

(d) south and east face

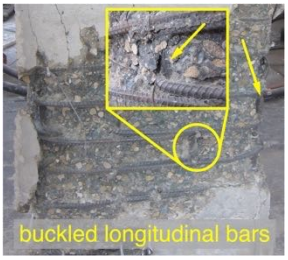

(e) damage on west face

(f) damage on south face

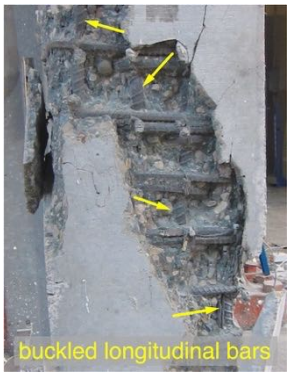

(g) damage on north face

(h) damage on east face

Figure 3.20 Damage patterns for specimen CWT-RT-N-80-10-#6

3.3 Data Reduction Procedure

The measured data were processed to obtain key parameters for comparing the performance of different specimens. The procedures for reducing the data are described in this section. Data reduction was performed by a series of bespoke RStudio (RStudio Team, 2021) scripts.

3.3.1 Average concrete strain

The applied load was recorded by the control system of the Southwark-Emery Testing Machine. Displacement was measured along the middle two-thirds of the central test region with LVDTs mounted to each face of the test specimen, resulting in a total of four LVDTs per specimen. It was assumed that failure would occur in the central test region. The LVDT displacements were divided by the measured gage lengths to obtain average concrete strain. When the LVDT data appeared to be accurate, the average displacement was calculated by averaging the results from all four LVDTs. A LVDT reading was removed from the average when data became erroneous or incorrect, which occasionally occurred due to concrete spalling or damage where the LVDT plate or wire was connected to the specimen. All LVDT data were

neglected at the conclusion of testing and while the testing machine head was being lifted away from the test specimens.

3.3.2 Reinforcement stress

Strain gage measurements were most accurate up to the peak load. Post-peak strain gage data were limited. The strain for gages on transverse and longitudinal reinforcement was determined by taking the average of the readings from all working strain gages. The contribution of a strain gage was removed if data became erroneous, which usually was marked by strain suddenly jumping to a large positive or negative value at or above the tensile fracture strain. Such jumps often happened near or soon after the peak load. The large jumps could indicate buckling in the longitudinal reinforcement or fracture in the transverse reinforcement, or just indicate that the longitudinal gage had gone "bad". Transverse and longitudinal average strain data are reported up to the point where the readings were available. The "cleaned" data were then averaged to obtain the average strains. The Ramberg-Osgood function (Eq. 3.1) was subsequently utilized to obtain average stress. The selected values of A, B, and C for various reinforcement used in this project are provided in Table 3.1. The strain (and hence stress) data at the conclusion of loading were excluded.

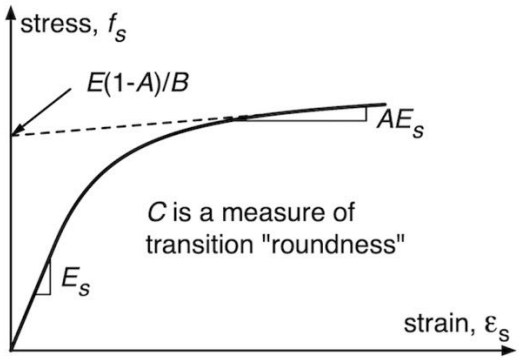

$$f_s = E_s \varepsilon_s \left\{ A + \frac{1 - A}{[1 + (B\epsilon_s)^C]^{1/C}} \right\} \leq f_u \qquad \text{Eq. 3.1}$$

Table 3.1 Reinforcement Ramberg-Osgood coefficients

Phase	Size	Grade	Supplier	Ramberg-Osgood Coefficients		
				A	B	C
1	No. 4	A706 Grade 60	1	0.02	390	2.80
	No. 4	A706 Grade 60	2	0.03	435	2.80
	No. 4	A706 Grade 80	2	0.03	270	2.91
	No. 4	A706 Grade 80	3	0.04	330	3.00
	No. 5	A706 Grade 60	1	0.03	340	2.50
	No. 5	A706 Grade 80	4	0.01	287	100
2	No. 4	A706 Gr. 60	5	0.01	377	3.9
	No. 4	A706 Gr. 80	5	0.023	300	2.75
	No. 5	A706 Gr. 60	5	0.00001	401	9.5
	No. 5	A706 Gr. 80	5	0.00001	317	14
	No. 6	A707 Gr. 60	5	0.002	386	45
	No. 6	A706 Gr. 80	5	0.002	386	45

3.3.3 Confined concrete properties

To obtain confined concrete stress, f'_{cc}, the contribution of the longitudinal reinforcement needed to be determined first. Using the average longitudinal reinforcement strain from strain gages, the corresponding stress was inferred from Ramberg-Osgood function. The resulting stress multiplied by the total area of longitudinal reinforcement is the force resisted by the longitudinal reinforcement. The confined concrete core stress was then calculated by dividing the total concrete contribution (total axial load minus the contribution of longitudinal reinforcement) by the concrete core area, defined as the area bound by the centerline of perimeter transverse reinforcement. A stress data point corresponding to $0.85f'_{cc}$ was generally not available. The closest available data point was used to determine ε_{85}.

Longitudinal reinforcement strain gage data are not available for first phase specimens CON-SQ-Y-80-10-#5 and CWT-SQ-Y-80-10-#5 after the peak load. To calculate f'_{cc} after the peak for these two specimens, the steel stress was assumed to plateau at the stress corresponding to the last strain gage reading. The assumption was found to be in good agreement with what was observed for the other specimens. In the case of second phase specimens, a different procedure was followed. For the last 500 data points before losing strain gage data, the ratio of strain gage value to the corresponding (i.e., for the same load) average strain determined from LVDTs was computed. After losing strain gage data, the average of these ratios was multiped by LVDT average strain to approximate longitudinal reinforcement strain gage data needed to calculate f'_{cc}.

3.4 Evaluation of Measured Data

The measured data are evaluated to examine the effects of (a) type of confinement: conventional versus CWT; (b) grade of reinforcement: Gr. 60 versus Gr. 80; (c) lateral support of longitudinal reinforcement: all bars are supported or some bars are not supported while meeting the ACI requirements ACI 18.10.6.4(f), i.e., "*Transverse reinforcement shall be configured such that the spacing h_x between laterally supported longitudinal bars around the perimeter of the boundary element shall not exceed the lesser of 14 in. and two-thirds of the boundary element thickness.*"; (d) whether the specimen is complaint with all the ACI requirements or not; (e) concrete compressive strength: 6 ksi versus 10 ksi; and (f) shape of the test specimen: rectangular versus square. The data acquisition computer malfunctioned during testing of specimen CWT-RT-N-80-10-#5 and, as a result, the data are not available for this specimen.

The following metrics are used to compare comparable specimens:

(a) P_{max}/P_o where P_{max} is the maximum measured axial load and P_o is the calculated axial load capacity using the measured material properties and without any reduction factors, i.e., $P_o = 0.85f'_c\left(A_g - A_{st}\right) + f_y A_{st}$.

(b) f_{tie}/f_{yt} where f_{tie} is the maximum experimentally inferred stress in transverse reinforcement and f_{yt} is the measured yield strength.

(c) f'_{cc}/f'_c where f'_{cc} is the maximum value of experimentally obtained confined concrete stress and f'_c is the measured concrete strength.

(d) ε_{85} which is the strain corresponding to experimentally obtained $0.85f'_{cc}$

3.4.1 Conventional versus Continuously Wound Ties

Normalized axial load (P_{max}/P_o) versus average strain is shown in Figure 3.21 for various specimens in which the type of transverse reinforcement was the only variable. The specimens with CWT generally exhibited better post-peak ductility, which is also seen from Figure 3.22 that indicates more ε_{85} values for CWT specimens are above the 45-degree line. The values in Table 3.2 indicate the same trend. The average, maximum, and minimum values of ε_{85} for the specimens with CWT are larger than those using conventional ties. The 95% confidence range of ε_{85} is 0.005 to 0.009 for the specimens reinforced with conventional ties in comparison to 0.011 to 0.0140 for those with CWT. Out of seven comparable specimens, the values of P_{max}/P_o and f_{tie}/f_{yt} are larger in four and six specimens using CWT, respectively. On average P_{max}/P_o is nearly the same for both types of transverse reinforcement (1.13 for conventional and 1.14 for CWT), and the 95% confidence range is also nearly the same: 1.08 to 1.18 for conventional ties versus 1.09 to 1.18 for CWT. The tie stress (f_{tie}/f_{yt}) in CWT is higher than conventional ties – average: 0.84 versus 0.71 and 95% confidence range: 0.64 to 1.03 versus 0.49 to 0.93. The larger normalized tie stresses indicate CWT could be engaged more than conventional ties. In three specimens, the value of f'_{cc}/f'_c is essentially not affected by the type of transverse reinforcement, and it is larger for two specimens with conventional ties but larger in two other specimens using CWT . The average values and the 95% confidence range for f'_{cc}/f'_c are larger for conventional ties: 1.22 versus 1.19 and 1.18 to 1.27 versus 1.14 to 1.24, respectively.

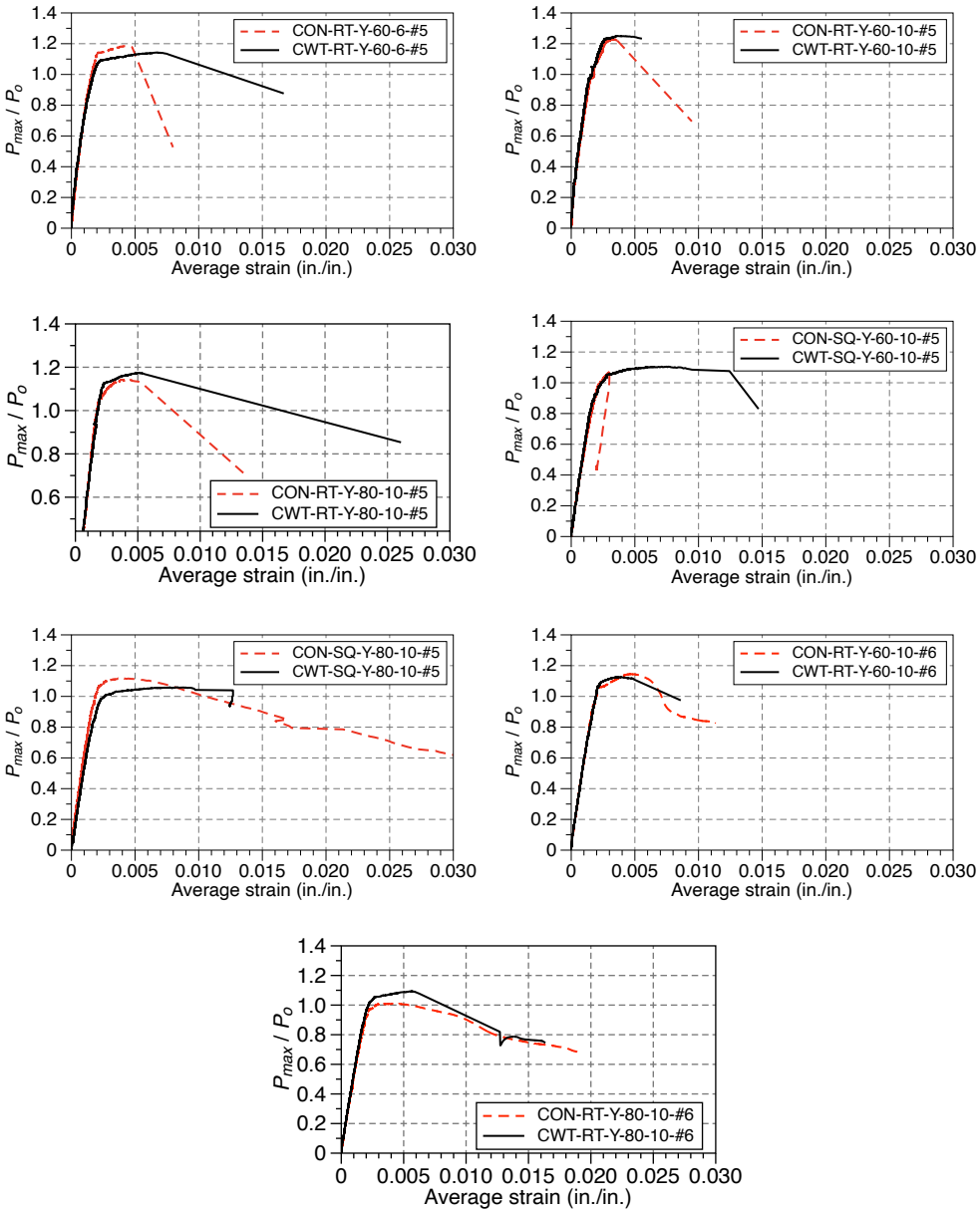

Figure 3.21 Normalized axial force versus average strain – convectional versus CWT

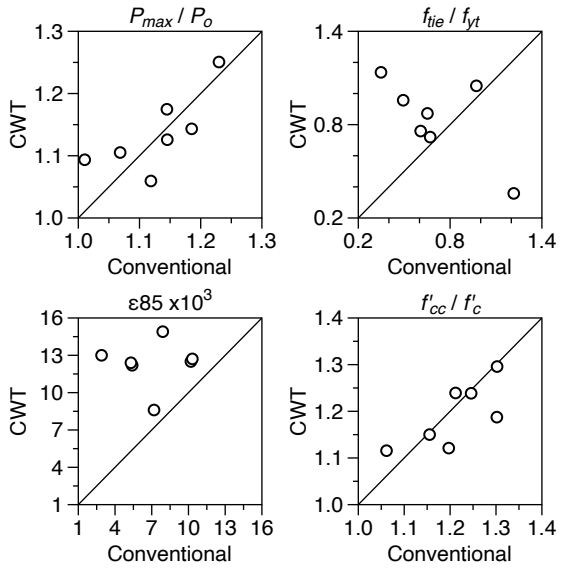

Figure 3.22 Effect of transverse reinforcement

Table 3.2 Comparison metrics for conventional and CWT

	P/P_o		f_{tie}/f_{yt}		ε_{85}		f_{cc}/f'_c	
	Conv.	CWT	Conv.	CWT	Conv.	CWT	Conv.	CWT
Average	1.13	1.14	0.708	0.836	0.0070	0.0123	1.22	1.19
Maximum	1.23	1.25	1.22	1.14	0.0103	0.0149	1.30	1.30
Minimum	1.01	1.06	0.348	0.358	0.00290	0.00860	1.15	1.12
COV	0.0644	0.0550	0.415	0.309	0.387	0.152	0.0514	0.0571
95% confidence range	1.08 to 1.18	1.09 to 1.18	0.49 to 0.93	0.64 to 1.03	0.005 to 0.009	0.011 to 0.014	1.18 to 1.27	1.14 to 1.24

3.4.2 Grade of reinforcement

Larger ductility of specimens using Gr. 80 is evident from normalized axial load (P_{max}/P_o) versus average strain shown in Figure 3.23 (a larger strain could be achieved before failure), Figure 3.24 (five data points are above the 45-degree equal line), and the values in Table 3.3 (e.g., the 95% confidence interval of ε_{85} for Gr. 80 is 0.009 to 0.013 versus 0.006 to 0.013 for Gr. 60, or the average ε_{85} is 0.011 and 0.009 for Gr. 80 and Gr. 60, respectively). However, five out of seven values of P_{max}/P_o are larger for Gr. 60 and one is not essentially affected by the grade of reinforcement; five out of seven values of f'_{cc}/f'_c are larger for Gr. 60, and the number of cases with a larger f_{tie}/f_{yt} is nearly divided equally between Gr. 60 and Gr. 80 (three for Gr. 60 and four for Gr. 80). Except for post-peak ductility (ε_{85}), a clear trend could not be identified about whether the specimens with CWT benefit more by using Gr. 60 or Gr. 80 reinforcement.

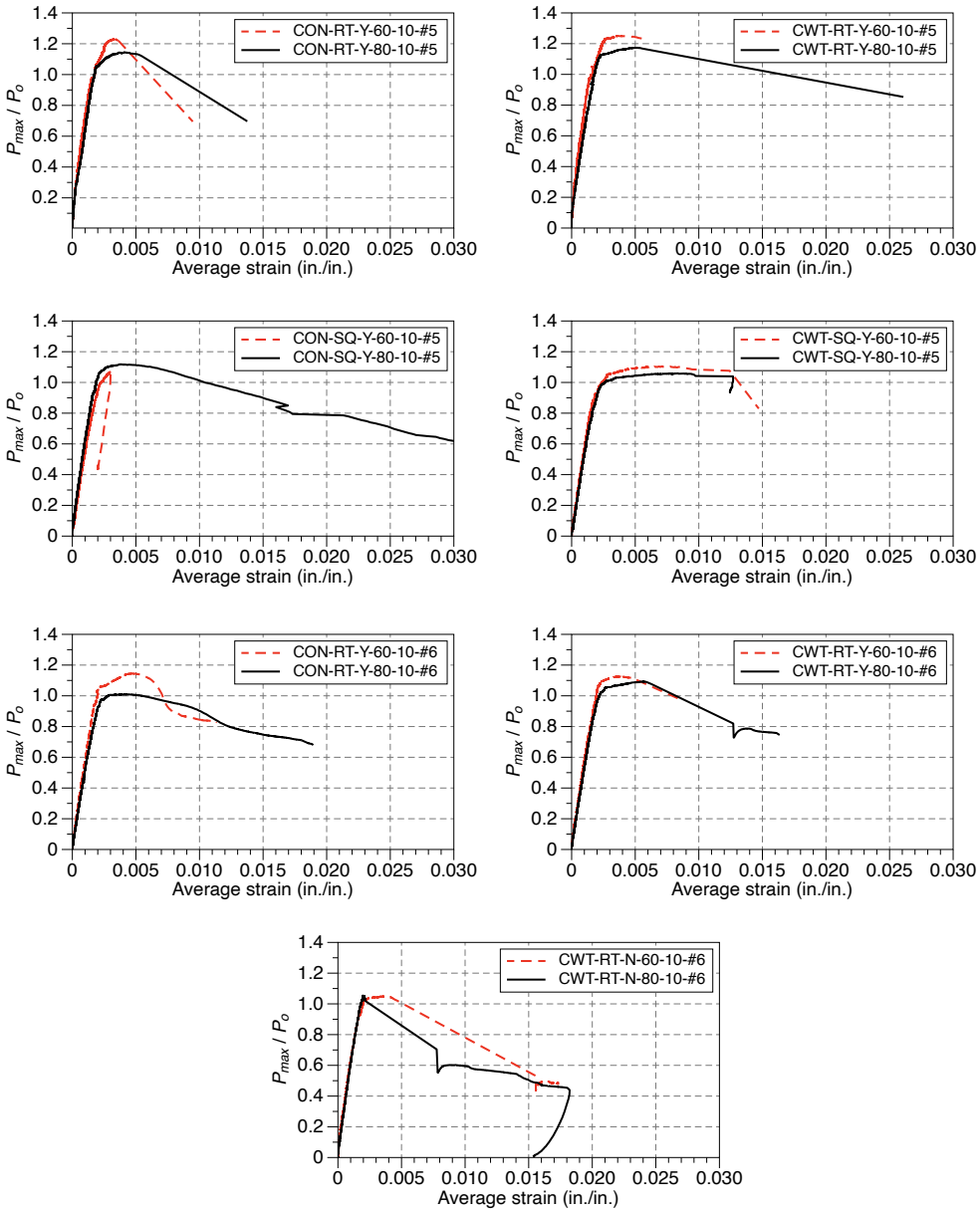

Figure 3.23 Normalized axial force versus average strain – Gr. 60 versus Gr. 80

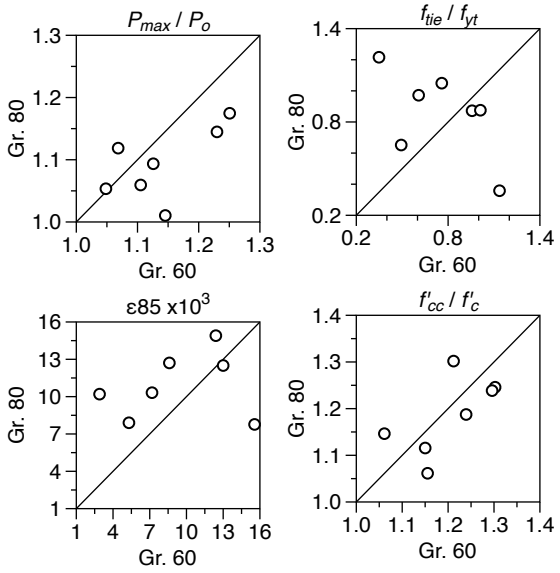

Figure 3.24 Effect of grade of reinforcement

Table 3.3 Comparison metrics for Gr. 60 and Gr. 80

	P/P_o		f_{tie}/f_{yt}		ε_{85}		f_{cc}/f'_c	
	Gr. 60	Gr. 80	Gr. 60	Gr. 80	Gr. 60	Gr. 80	Gr. 60	Gr. 80
Average	1.13	1.09	0.769	0.856	0.00928	0.0109	1.19	1.19
Maximum	1.25	1.17	1.14	1.22	0.0156	0.0149	1.30	1.30
Minimum	1.05	1.01	0.348	0.358	0.00290	0.00777	1.06	1.06
COV	0.0682	0.0522	0.352	0.327	0.491	0.241	0.0784	0.0704
95% confidence range	1.08 to 1.18	1.05 to 1.14	0.58 to 0.96	0.65 to 1.06	0.006 to 0.013	0.009 to 0.013	1.12 to 1.25	1.12 to 1.25

3.4.3 Lateral support of longitudinal bars

A total of six comparable specimens are evaluated to examine the impact of lateral support of longitudinal bars. The measured data are insufficient to obtain ε_{85} for specimen CWT-RT-N-60-10-#5; hence, only five values of ε_{85} could be compared. The specimens in which all the longitudinal bars were laterally supported have slightly larger post-peak ductility (Figure 3.25). As seen from Figure 3.26, three cases with lateral support for all the longitudinal bars have a larger value of ε_{85}. Ductility in terms of the value of ε_{85} is marginally larger when all the longitudinal bars are supported. The values in Table 3.4 show the maximum value of ε_{85} is 0.0104 by providing lateral support for all the longitudinal bars, and it is 0.00985 if some of the bars were not laterally supported. The 95% confidence range is essentially unchanged: 0.008 to 0.013 (all bars are laterally supported) and 0.007 to 0.013 (some bars are not laterally supported). The other three metrics suggest conflicting trends; the average values of P_{max}/P_o and f'_{cc}/f'_c are larger for the cases with not all the longitudinal bars being supported, but on average f_{tie}/f_{yt} is larger by providing lateral support to all the longitudinal bars.

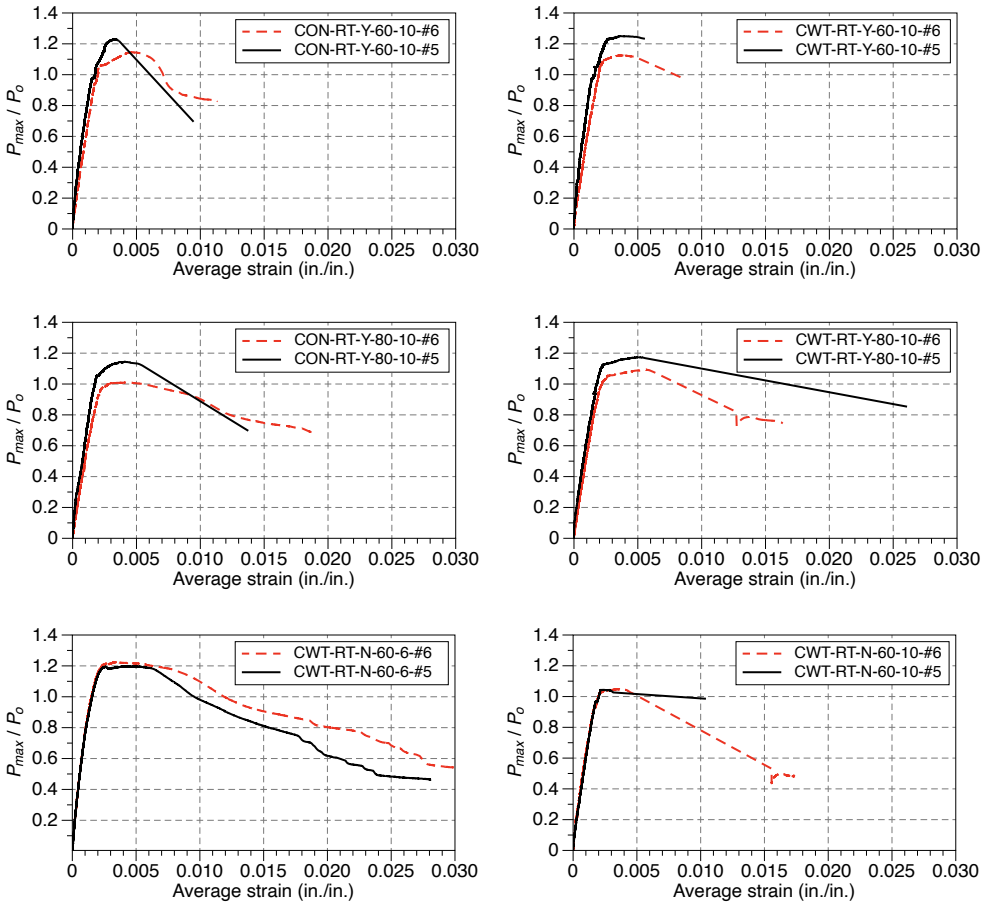

Figure 3.25 Normalized axial force versus average strain – lateral support of longitudinal bars

(All the longitudinal bars were supported for the specimens using #6)

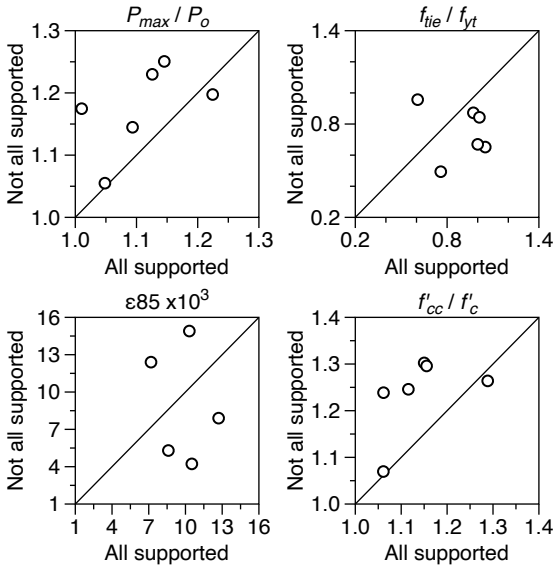

Figure 3.26 Impact of lateral support of longitudinal bars

Table 3.4 Comparison metrics for all longitudinal bars are supported or not

	P/P_o		f_{tie}/f_{yt}		ε_{85}		f_{cc}/f'_c	
	All	Not all	All	Not all	All	Not all	All	Not all
Average	1.10	1.18	0.896	0.748	0.0104	0.00985	1.14	1.24
Maximum	1.22	1.25	1.05	0.957	0.0156	0.0149	1.29	1.30
Minimum	1.01	1.05	0.608	0.494	0.00719	0.00530	1.06	1.07
COV	0.0655	0.0596	0.180	0.230	0.285	0.385	0.0674	0.0692
95% confidence range	1.05 to 1.15	1.12 to 1.23	0.78 to 1.02	0.61 to 0.89	0.008 to 0.013	0.007 to 0.013	1.08 to 1.2	1.17 to 1.3

3.4.4 Compliance with ACI transverse reinforcement requirements

All five comparable specimens for this comparison utilized CWT. The available data are inadequate to determine ε_{85} for specimens CWT-RT-Y-60-10-#5 and CWT-RT-Y-80-10-#5. As mentioned previously, the data for CWT-RT-N-80-10-#5 are not available. The measured data (Figure 3.27, Figure 3.28, and Table 3.5) indicate a better performance was achieved by satisfying the ACI requirements for transverse reinforcement. For instance, 95% confidence range for ε_{85} is 0.011 to 0.014 when the specimens met all the ACI requirements versus 0.006 to 0.015 when they did not, the maximum value of f'_{cc}/f'_c is increased by 3.5% (1.18 versus 1.14) when the specimens were ACI compliant, or meeting ACI requirements resulted in about 6.4% increase in average value of P_{max}/P_o (1.16 versus 1.09). Except for f'_{cc}/f'_c, the comparison metrics are larger for more cases that are compliant with ACI transverse reinforcement requirements than those that are not.

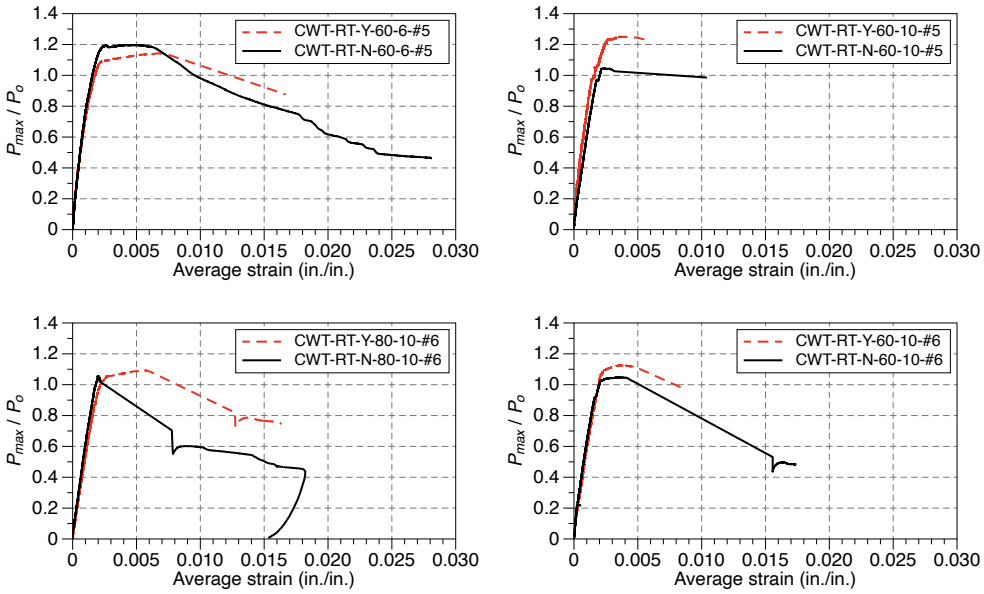

Figure 3.27 Normalized axial force versus average strain – compliance versus noncompliance

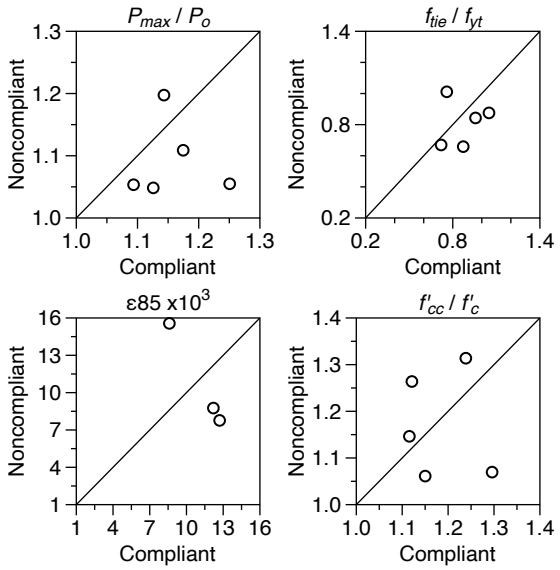

Figure 3.28 Impact of compliance with ACI transverse reinforcement requirements

Table 3.5 Comparison metrics for compliance with ACI transverse requirements

	P/P_o		f_{tie}/f_{yt}		ε_{85}		f_{cc}/f'_c	
	Yes	No	Yes	No	Yes	No	Yes	No
Average	1.16	1.09	0.871	0.850	0.0122	0.01070	1.18	1.14
Maximum	1.25	1.20	1.049	1.011	0.0149	0.01556	1.30	1.26
Minimum	1.09	1.05	0.720	0.669	0.0086	0.00777	1.12	1.06
COV	0.0516	0.0667	0.157	0.165	0.186	0.3968	0.0671	0.0827
95% confidence range	1.11 to 1.21	1.02 to 1.16	0.75 to 0.99	0.71 to 0.99	0.01 to 0.014	0.006 to 0.015	1.11 to 1.25	1.04 to 1.23

3.4.5 Concrete compressive strength

The measured data are not sufficient to determine ε_{85} in specimen CWT-RT-N-60-10-#5. The available data are illustrated in Figure 3.29 and Figure 3.30 and summarized in Table 3.6. The average values of f_{tie}/f_{yt} and ε_{85} for 10-ksi specimens are larger than their counterparts using 6 ksi concrete (8% and 20%, respectively). However, P_{max}/P_o and f'_{cc}/f'_c are marginally larger for the specimens using 6 ksi concrete (3.5% and 3.4%, respectively). No clear trend could be identified about whether CWT benefits by using high strength concrete (nominal 10 ksi) instead of normal strength concrete (nominal 6 ksi).

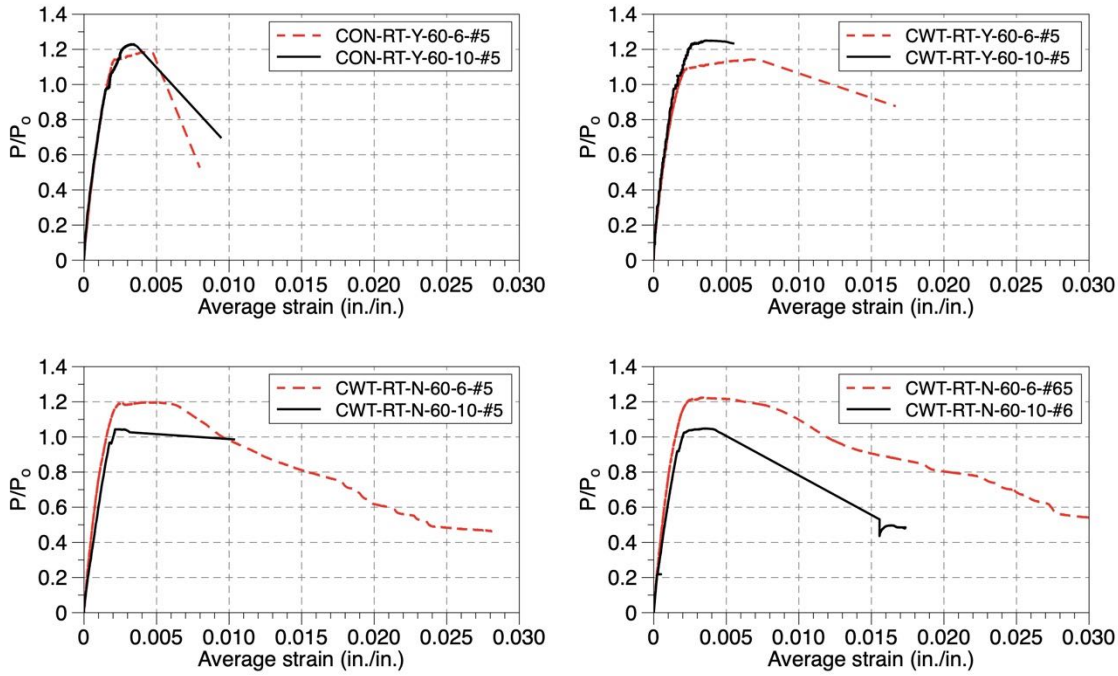

Figure 3.29 Normalized axial force versus average strain – concrete compressive strength

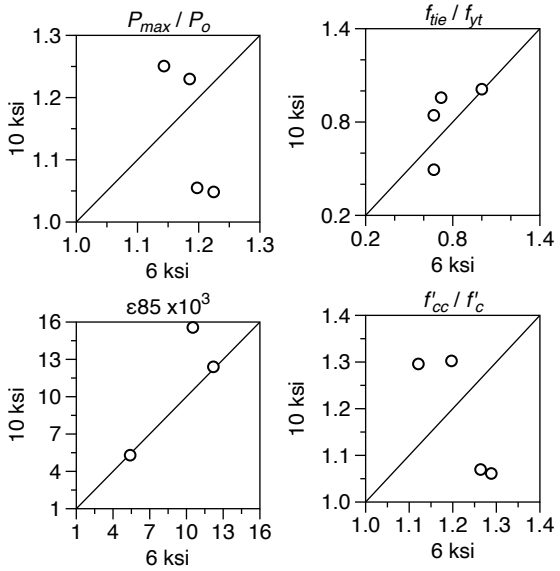

Figure 3.30 Impact of concrete compressive strength

Table 3.6 Comparison metrics for concrete compressive strength

	P/P_o		f_{tie}/f_{yt}		ε_{85}		f_{cc}/f'_c	
	6 ksi	10 ksi	6 ksi	10 ksi	6 ksi	10 ksi	6 ksi	10 ksi
Average	1.19	1.15	0.765	0.826	0.00922	0.01109	1.22	1.18
Maximum	1.22	1.25	1.000	1.011	0.0122	0.0156	1.29	1.30
Minimum	1.14	1.05	0.669	0.494	0.00540	0.00530	1.12	1.06
COV	0.0285	0.0953	0.2074	0.281	0.315	0.474	0.0616	0.114

3.4.6 Shape of boundary element

Out of four comparable specimens, two rectangular specimens exhibited larger ductility (i.e., larger ε_{85}) than their square counterparts and two square specimens showed opposite trends (Figure 3.31 and Figure 3.32). All four rectangular specimens developed a larger capacity than the square specimens – the average value of P_{max}/P_o being 1.20 and 1.09 (10.3% difference) for rectangular and square specimens, respectively (see

Table 3.7). Normalized confined concrete strength (f'_{cc}/f'_c) is larger in three rectangular specimens, but on average it is only 2.9% larger than that for the square columns. The larger value of f_{tie}/f_{yt} is evenly divided between the two shapes, but the average value of square specimens is larger by 2.8% (0.765 versus 0.744).

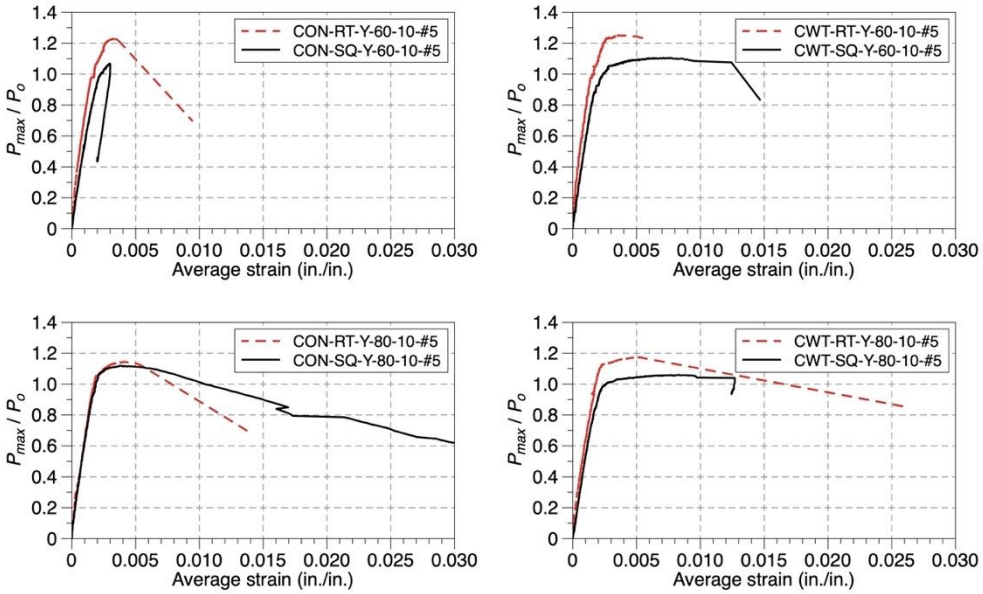

Figure 3.31 Normalized axial force versus average strain - shape

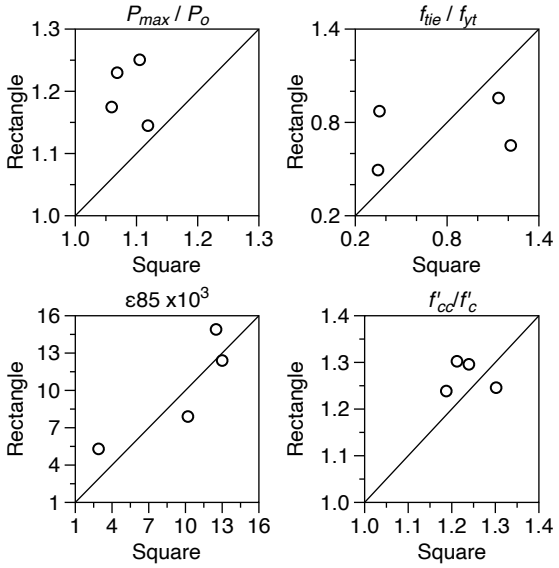

Figure 3.32 Impact of shape

Table 3.7 Comparison metrics for shape of specimen

	P_{max}/P_o		f_{tie}/f_{yt}		ε_{85}		f'_{cc}/f'_c	
	Rect.	Sq.	Rect.	Sq.	Rect.	Sq.	Rect.	Sq.
Average	1.20	1.09	0.744	0.765	0.0101	0.00965	1.27	1.24
Maximum	1.25	1.12	0.957	1.22	0.0149	0.0130	1.30	1.30
Minimum	1.14	1.06	0.494	0.348	0.00530	0.00290	1.24	1.19
COV	0.0407	0.0262	0.283	0.623	0.428	0.483	0.0260	0.0399

The number of available data points was deemed inadequate to determine 95% confidence range.

3.5 Evaluation of Confined Concrete Models

Using the measured material properties and as-built dimensions, confined concrete stress-strain relationships were determined using (a) Saatcioglu and Razvi (1992), (b) Razvi and Saatcioglu (1998), and (c) Mander et al. (1988), which were discussed in Chapter 1. The results from these models are plotted against their experimentally obtained counterparts in Figure 3.33 and Figure 3.34. Furthermore, experimentally obtained peak compressive concrete compressive strength (f'_{cc}) and strain at 85% of peak compressive strength (ε_{85}) are compared against the values from the models, see Figure 3.35.

All the models tend to overestimate ε_{85}. For example, the measured ε_{85} for the specimens with CWT is on average 0.614 times the value determined from Razvi and Saatcioglu (1998) and the corresponding ratio is 0.346 for conventionally reinforced specimens – see Table 3.8. The same trend is observed for the other two models, but these two models tend to overestimate ε_{85} more, i.e., the ratios shown in Table 3.8 are smaller. If all the specimens are considered, the differences between the three models in terms of predicting post-peak stiffness become less.

The models predict f'_{cc} better than ε_{85}. On average the experimental f'_{cc} (normalized with respect to f'_c) is 1.006 and 0.985 times the values from Saatcioglu and Razvi (1992) for the specimens using conventional ties and CWTs, respectively. If all the specimens are considered, with 95% confidence the mean measured f'_{cc}/f'_c is between 0.968 and 1.029 times what Saatcioglu and Razvi (1992) predicts. The other two models overestimate f'_{cc}/f'_c more. Considering all the specimens, the measured/calculated magnitude of f'_{cc}/f'_c is on average 0.897 and 0.840 for Razvi and Saatcioglu (1998) and Mander et al. (1988), respectively versus 0.998 for Saatcioglu and Razvi (1992).

A clear explanation for the noticeable differences between the measured post-peak behavior (ε_{85}) and those from the models could not be identified. A plausible reason could be the models have been developed mostly based on the experimental data from specimens that were shorter (18 in. to 47 in.) than the test specimens (72 in.). The uniformity of concrete strength is reduced as the specimen height increases. Another reason could be due to the differences in the aggregates used in the test specimens versus those in the specimens that are basis of the models. Aggregate surface roughness affects tension stiffening.

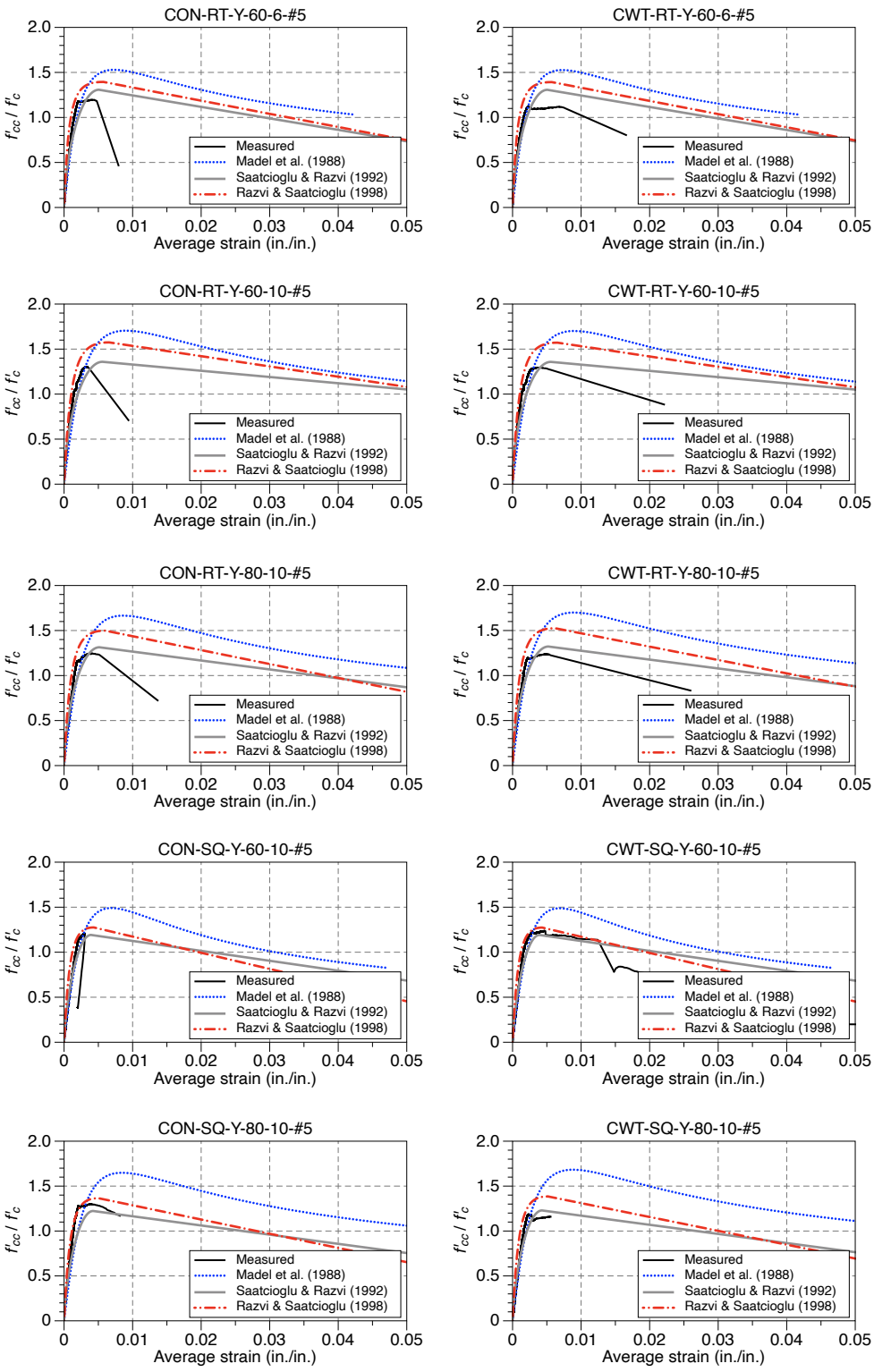

Figure 3.33 Concrete stress-strain relationships – experimental versus various models (phase 1)

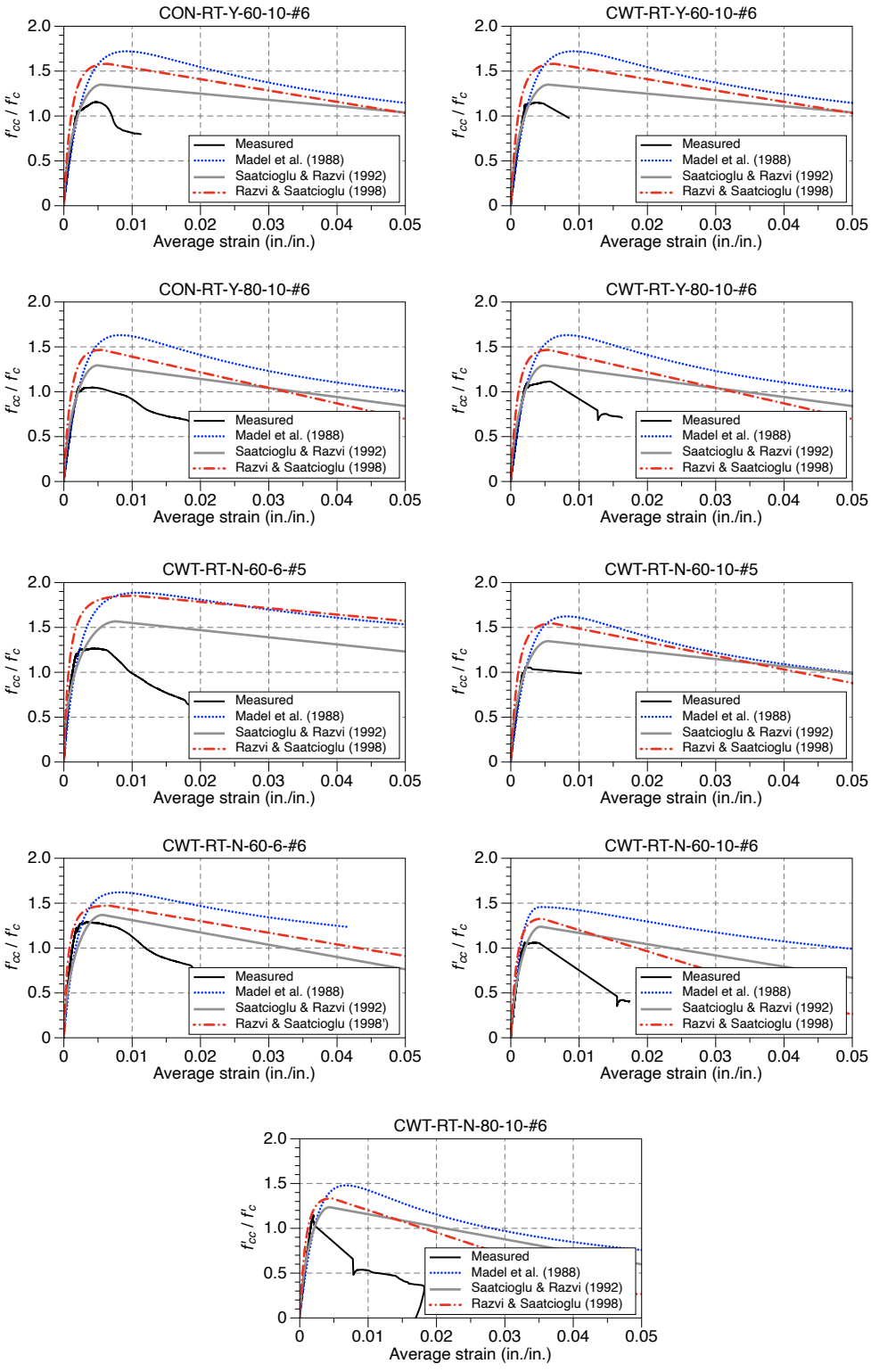

Figure 3.34 Concrete stress-strain relationships – experimental versus various models (phase 2)

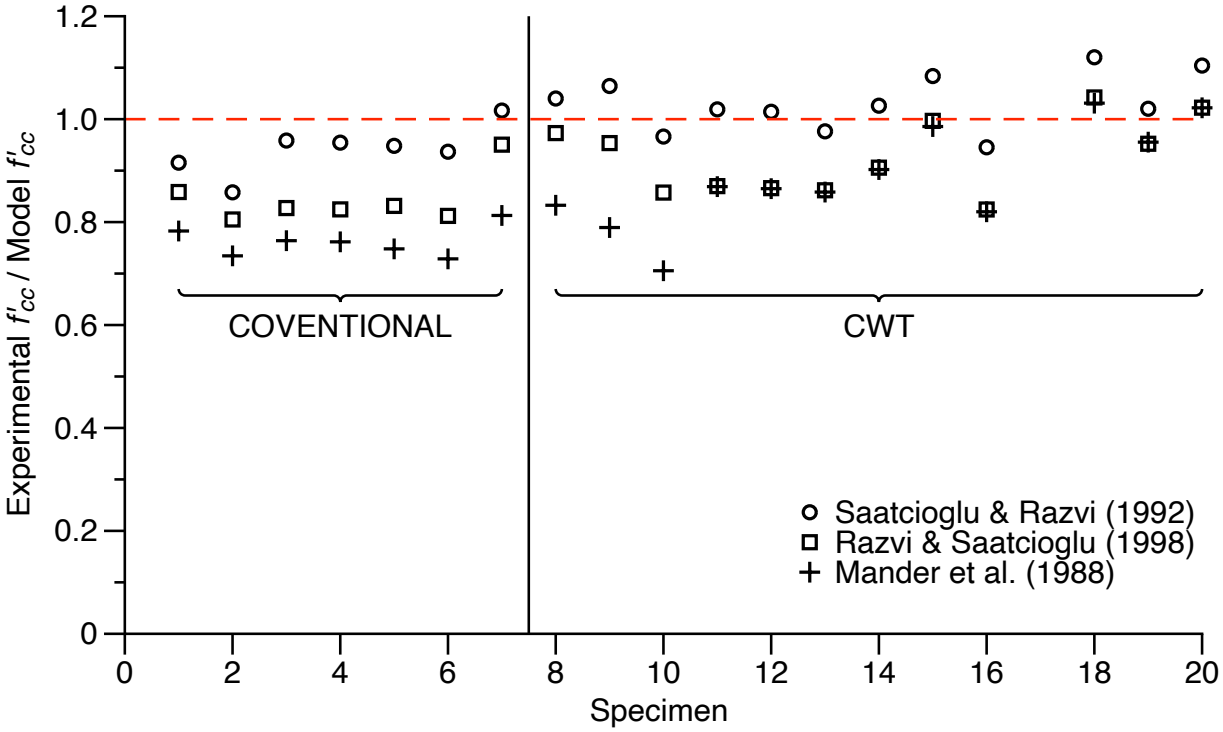

(a) Peak compressive strength (f'_{cc})

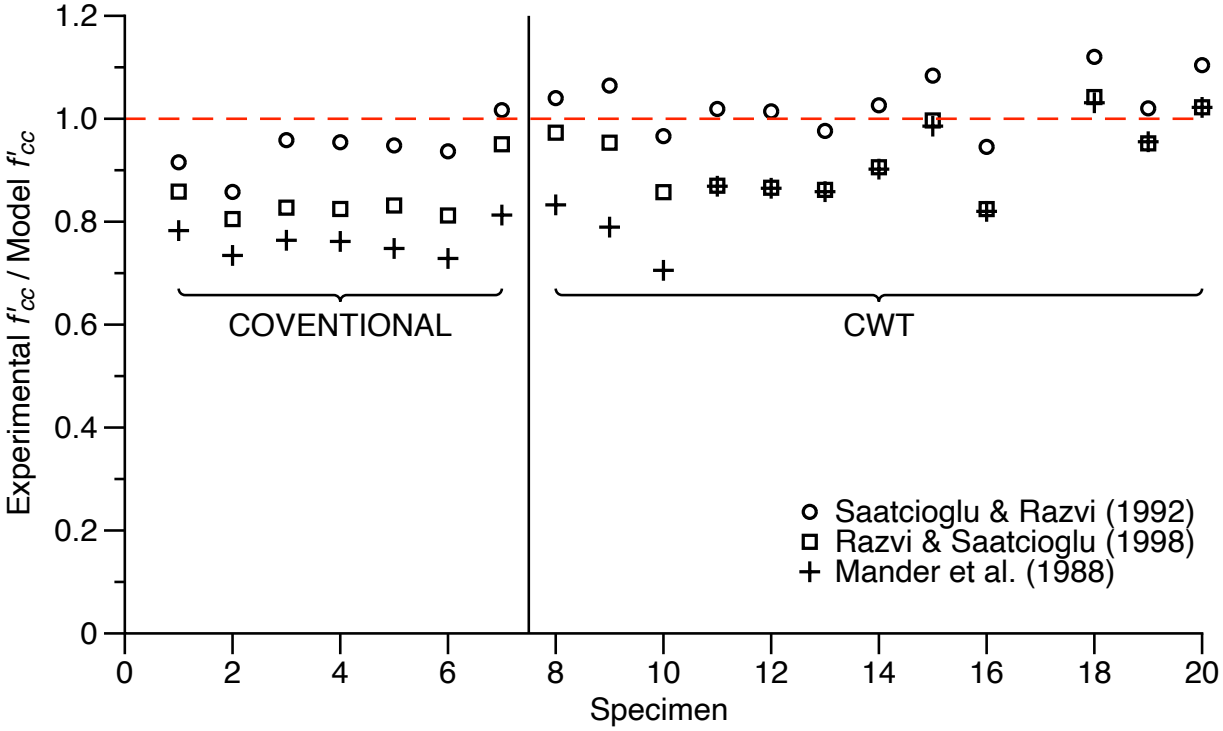

(b) Strain at 85% of peak stress (ε_{85})

Figure 3.35 Experimental values of f'_{cc} and ε_{85} versus the values from various models

Table 3.8 Comparison of key parameters of confined concrete

Conventional ties

	ε_{85} (measured/calculated)			f_{cc}/f'_c (measured/calculated)		
	Sattacigolou 1992	Sattacigolou 1998	Mander 1988	Sattacigolou 1992	Sattacigolou 1998	Mander 1988
Average	0.277	0.346	0.288	0.985	0.879	0.803
Maximum	0.459	0.570	0.449	1.064	0.954	0.869
Minimum	0.144	0.193	0.176	0.915	0.827	0.748
COV	0.446	0.452	0.337	0.051	0.059	0.057
95% confidence range	0.185 to 0.368	0.23 to 0.461	0.216 to 0.359	0.948 to 1.023	0.84 to 0.918	0.769 to 0.837

CWT

	ε_{85} (measured/calculated)			f_{cc}/f'_c (measured/calculated)		
	Sattacigolou 1992	Sattacigolou 1998	Mander 1988	Sattacigolou 1992	Sattacigolou 1998	Mander 1988
Average	0.502	0.614	0.484	1.006	0.907	0.862
Maximum	0.770	1.143	0.793	1.120	1.042	1.031
Minimum	0.236	0.318	0.204	0.858	0.805	0.705
COV	0.301	0.395	0.416	0.077	0.096	0.136
95% confidence range	0.413 to 0.592	0.47 to 0.757	0.365 to 0.604	0.962 to 1.049	0.858 to 0.956	0.796 to 0.928

All specimens

	ε_{85} (measured/calculated)			f_{cc}/f'_c (measured/calculated)		
	Sattacigolou 1992	Sattacigolou 1998	Mander 1988	Sattacigolou 1992	Sattacigolou 1998	Mander 1988
Average	0.414	0.510	0.408	0.998	0.897	0.840
Maximum	0.770	1.143	0.793	1.120	1.042	1.031
Minimum	0.144	0.193	0.176	0.858	0.805	0.705
COV	0.429	0.486	0.472	0.068	0.084	0.119
95% confidence range	0.332 to 0.497	0.395 to 0.624	0.319 to 0.497	0.968 to 1.029	0.863 to 0.931	0.796 to 0.885

Chapter 4 Summary and Conclusions

4.1 Summary

Continuously wound ties (CWTs) offer advantages over conventional transverse reinforcement in terms of construction speed. CWTs are also expected to provide a higher level of confinement than conventional transverse reinforcement because most legs of CWTs do not rely on the development length of hooked bars. The performance enhancements are especially beneficial to special seismic systems, specifically columns of special moment frames and special boundary elements (SBEs) of walls. The current ACI 318 code considers CWTs the same as conventional transverse reinforcement. The reported research was conducted to (a) identity potential strength and strain capacity enhancements from using CWTs and (b) compare stress-strain relationships of concrete confined by CWTs (and conventional ties) with widely used models.

The main goal of this project was to compare the performance of CWTs to conventional transverse reinforcement as confinement reinforcement. Specimens were designed per ACI 318-19 provisions for SBEs. A total of twenty reduced-scale specimens were designed, tested, and evaluated in terms of strength and ductility. The following variables were investigated: (a) type of tie (conventional or CWT), (b) reinforcement yield strength (ASTM A706 Grade 60 or ASTM A706 Grade 80), (c) specified strength of concrete (6000 psi or 10000 psi), (d) lateral support of longitudinal bars (every bar or every other bar is supported), (e) ACI transverse reinforcement requirements (compliant or noncompliant), (f) shape of cross section (square or rectangle). The research was conducted in two phases with the results and observations from the first phase informing the selection of the test variables for the second phase specimens.

4.2 Observations and conclusions

Based on the presented data, the following conclusions are drawn. The conclusions are grouped in terms of the key test variables and comparisons against confined concrete models.

4.2.1 Conventional ties versus CWT

1. All specimens were tested to ultimate loads (P_{max}) that exceeded ACI axial compressive strength capacity at zero eccentricity (P_o) without any reduction factors. As expected, the type of confinement did not noticeably affect the compressive strength: with 95% confidence, the mean value of P_{max}/P_o is between 1.08 and 1.18 (i.e., 95% confidence range) for conventional ties and it is between 1.09 and 1.18 for CWTs.

2. The specimens confined with CWTs exhibited improved post-peak ductility in comparison to those employing conventional ties. The post-peak ductility was assessed in terms of ε_{85}, which is the strain corresponding to 85% of the peak confined concrete stress. The average value of ε_{85} is increased by 75% by using CWT (0.0123 for CWT vs. 0.0070 for conventional ties). Additionally, the 95% confidence range of ε_{85} is increased substantially from 0.005-0.009 for the specimens with conventional ties to 0.011-0.014 when CWT is used.

3. The influence of CWT is less noticeable in terms of the maximum tie stress and confined concrete stress.

4.2.2 Grade of reinforcement

1. The largest impact of reinforcement grade is on the post-peak ductility. With 95% confidence, the mean value of ε_{85} is 0.009 to 0.013 for the specimens using Gr. 80 reinforcement in comparison to 0.006 to 0.013 for those with Gr. 60 reinforcement. On average, the value of ε_{85} is increased by 18% by utilizing Gr. 80 reinforcement.

2. To a lesser degree, the grade of reinforcement influenced transverse reinforcement stress. The ties with Gr. 80 reinforcement reached a maximum stress of $1.22f_{yt}$ in comparison to $1.14f_{yt}$ for those employing Gr. 60 reinforcement.

3. The maximum confined concrete strength is unchanged. The average value of f'_{cc}/f'_c is 1.19 for Gr. 60 and Gr. 80.

4.2.3 Compliance with ACI transverse reinforcement requirements

1. Compliance with current ACI transverse reinforcement requirements could only be evaluated with reference to CWTs. Not meeting the ACI requirements had a deleterious effect on all the selected comparison metrics (P_{max}/P_o, f_{tie}/f_{yt}, f'_{cc}/f'_c, and ε_{85}).

2. The most noticeable negative impact is on ε_{85}, which on average is reduced by nearly 12% if the CWTs do not meet ACI transverse reinforcement requirements. The maximum axial load and peak concrete compressive strength are lowered by about 6% and 4%, respectively. The normalized transverse reinforcement stress in the noncompliant specimens is on average approximately 3% less than their counterpart compliant specimens.

4.2.4 Lateral support of longitudinal reinforcement

1. The spacing between longitudinal bars met ACI requirements regardless of if all the bars were supported (case A) or not (case B). The latter specimens had seven longitudinal bars on each long face (three of which were not supported) versus four for the former cases. Both cases had the same number of longitudinal bars on the short faces. The larger number of longitudinal bars for case B resulted in a more uniform confining pressure which led to lager confined concrete strength than what could be achieved for case A. The more uniform confining pressure is expected to also enhance post-peak ductility, but the measured data do not support this trend (ε_{85} for case A specimens is larger than the value for case B specimens). The reason for this discrepancy is unclear.

2. It is important to satisfy ACI spacing limits for longitudinal bars.

4.2.5 Concrete compressive strength and specimen shape

1. The most appreciable beneficial effect of higher concrete strength is for ε_{85}, which on averaged increased by 20%, followed by an increase of 8% for f_{tie}/f_{yt}. However, the average values of P_{max}/P_o and f'_{cc}/f'_c were smaller for the 10-ksi specimens in comparison to those using 6 ksi concrete (approximately 4% and 3% less, respectively). These reductions are attributed to the differences of failure patterns, e.g., whether damage was more dominant in the test region compared to the top or bottom.

2. Rectangular specimens had larger values of P_{max}/P_o, f'_{cc}/f'_c, and ε_{85} than their square counterparts. The opposite trend was observed for f_{tie}/f_{yt}.

4.2.6 Evaluation of concrete models

1. Regardless of the type of transverse reinforcement, Sattacigolou and Razvi (1992) predicts the confined concrete compressive reasonably well and better than the two other models considered in this study. With 95% confidence, the mean measured f'_{cc} for the specimens with conventional ties is 0.948 to 1.023 times the value determined from Sattacigolou and Razvi (1992). The corresponding values are 0.962 to 1.049 for CWT specimens.

2. All the models overpredict the post-peak ductility of confined concrete although Razi and Sattacigolou (1998) is slightly better particularly for CWT specimens. The average measured ε_{85} is 0.61 and 0.35 times the calculated values for the specimens with CWT and conventional ties, respectively. The corresponding values are 0.50 and 0.28 for Sattacigolou and Razvi (1992) and 0.48 and 0.29 for Mander et al. (1988).

4.3 Recommendations

1. All the current ACI requirements for transverse reinforcement must be satisfied to take full advantage of enhanced post-peak ductility offered by continuously wound ties. Moreover, it is recommended to use Gr. 80 continuously wound ties in conjunction with high strength concrete (10 ksi) to further enhance ductility.

2. The use of Sattacigolou and Razvi (1992) is recommended to obtain the expected compressive strength confined by continuously wound ties or conventional ties. The likely value of ε_{85} for either type of transverse reinforcement should be taken as one half of the value computed from Razi and Sattacigolou (1998).

References

ACI (American Concrete Institute) Committee 318. (2014). Building code requirements for structural concrete (ACI 318-14) and commentary (ACI 318-14R). Farmington Hills, MI.

ACI (American Concrete Institute) Committee 318. (2019). Building code requirements for structural concrete (ACI 318-19) and commentary (ACI 318-19R). Farmington Hills, MI.

Arteta, C. A., To, D. V., & Moehle, J. P. (2014). Experimental response of boundary elements of code-compliant reinforced concrete shear walls. Proceedings of the 10th National Conference in Earthquake Engineering, Anchorage, AK. pp. 1-1-15.

Arteta, C. A. (2015). Seismic response assessment of thin boundary elements of special concrete shear walls. Unpublished Doctor of Philosophy in Engineering - Civil and Environmental Engineering, University of California, Berkely, Berkely, CA.

ATC 115. (2014). Roadmap for the use of high-strength reinforcement in reinforced concrete design. Redwood City, CA: Applied Technology Council.

Behrouzi, A., Welt, T., Lehman, D., Lowes, L., LaFave, J., & Kuchma, D. (2017). Experimental and numerical investigation of flexural concrete wall design details. Structures Congress, Denver, Colorado. pp. 418-418-433.

Chang, G. A., & Mander, J. B. (1994). Seismic energy-based fatigue damage analysis of bridge columns: Part 1 - evaluation of seismic capacity No. NCEER-94-0006). Buffalo, NY: State University of New York.

Cusson, D., & Paultre, P. (1994). High-strength concrete columns confined by rectangular ties. Journal of Structural Engineering, 120(3), 783-783-804.

Gosh, S. K. (2016, Confinement of special reinforced concrete moment frame columns. STRUCTURE Magazine, 26-26-29.

Mander, J. B., Priestley, M. J. N., & Park, R. (1988). Observed stress-strain behavior of confined concrete. Journal of Structural Engineering, 114(8), 1827-1827-1849.

Mander, J. B., Priestley, M. J. N., & Park, R. (1988). Theoretical stress-strain model for confined concrete. Journal of Structural Engineering, 114(8), 1-1-23.

Massone, L. M., Polanco, P., & Herrera, P. (2014). Experimental and analytical response of RC wall boundary elements. Proceedings of the 10th National Conference in Earthquake Engineering, Earthquake Engineering Research Institute, Anchorage, AK.

Moehle, J. P. (1992). Displacement-based design of RC structures subjected to earthquakes. Earthquake Spectra, 8(3), 403-403-428.

Moehle, J. P., & Bavanagh, T. (1985). Confinement effectiveness of crossties in RC. Journal of Structural Engineering, 111(10), 2105-2105-2120.

RStudio Team (2021). RStudio: Integrated Development Environment for R. RStudio, PBC, Boston, MA URL http://www.rstudio.com/.

Popovics, S. (1973). A numerical approach to the complete stress-strain curve of concrete. Concrete and Cement Research, 3(5), 583-599.

Ramberg, W. and Osgood, W.R. (1943) Description of Stress-Strain Curves by Three Parameters, National Advisory Committee on Aeronautics, TN 902.

Razvi, S., & Saatcioglu, M. (1994). Strength and deformability of confined high-strength concrete columns. ACI Structural Journal, 91(6), 678-678-687.

Saatcioglu, M., & Razvi, S. R. (1992). Strength and ductility of confined concrete. Journal of Structural Engineering, 118(6), 1590-1590-1607.

Saatcioglu, M., & Razvi, S. R. (1998). High-strength concrete columns with square sections under concentric compression. Journal of Structural Engineering, 124(12), 1438-1438-1447.

Scott, B. D., Park, R., & Priestley, M. J. N. (1982). Stress-strain behavior of concrete confined by overlapping hoops at low and high strain rates. Journal of the American Concrete Institute, 79(1), 13-13-27.

Shahrooz, B. M., Forry, N. S. A., Bill, H. L., & Doellman, A. M. (2016). Continuous transverse reinforcement - behavior and design implications. ACI Structural Journal, 113(5), 1085-1085-1094.

Sharma, U. K., Bhargava, P., & Kaushik, S. K. (2005). Behavior of confined high strength concrete columns under axial compression. Journal of Advanced Technology, 3(2), 267-267-281.

Sheikh, S. A., Shah, D. V., & Khoury, S. S. (1994). Confinement of high-strength concrete columns. ACI Structural Journal, 91(1)

Sheikh, S. A., & Uzumeri, S. M. (1980). Strength and ductility of tied concrete columns. Journal of the Structural Division-ASCE, 106(5), 1079-1079-1102.

Welt, T. S. (2015). Detailing for compression in reinforced concrete wall boundary elements: Experiments, simulations, and design recommendations. Unpublished Ph.D. thesis, Univ. of Illinois, Urbana-Champaign, IL.

Welt, T. S., Massone, L. M., LaFave, J. M., & Lehman, D. E. (2017). Confinement behavior of rectangular reinforced concrete prisms simulating wall boundary elements. Journal of Structural Engineering, 143(4), 1-1-12